EUROPEAN ORGANIZATION FOR NUCLEAR RESEARCH

CERN/SPSC 98–4
CERN/SPSLC/P264 Add. 2
9 January 1998

ADDENDUM–2 to PROPOSAL SPSLC/P264

Status and Future Programme of the NA49 Experiment

J. Bächler[5], D. Barna[4], L.S. Barnby[3], J. Bartke[6], R.A. Barton[3], H. Bialkowska[14,5], A. Billmeier[10], C.O. Blyth[3], R. Bock[7], J. Bracinik[19], F.P. Brady[8], R. Brun[5] , P. Buncic[5,10], G.E. Cooper[2], J.G. Cramer[16], P. Csato[4], V. Eckardt[13], F. Eckhardt[12], T. Empl[20], J. Eschke[7], H.G. Fischer[5], D. Flierl[10], Z. Fodor[4], U. Frankenfeld[7], P. Foka[10,*], P. Freund[13], V. Friese[12], J. Ftacnik[19], F. Gabler[10], J. Gal[4], R. Ganz[13], M. Gaździcki[10], E. Gładysz[6], J. Grebieszkow[15], J.W. Harris[17], S. Hegyi[4], T. Henkel[12], V. Hlinka[19], M. Ivanov[19], G. Igo[11], R. Janik[19], P. Jacobs[2], P.G. Jones[3], K. Kadija[18,13], V.I. Kolesnikov[9], M. Kowalski[6], B. Lasiuk[17], P. Lévai[4], U. Lynen[7], A.I. Malakhov[9], S. Margetis[2,$], C. Markert[7], B. Mayes[20],G.L. Melkumov[9], J. Molnár[4], J.M. Nelson[3], M. Oldenburg[10], G. Odyniec[2], G. Palla[4], A.D. Panagiotou[1], Y. Pestov[7], A. Petridis[1], M. Pikna[19], L. Pinsky[20], R.J. Porter[2], A.M. Poskanzer[2], S. Poziombka[10], D.J. Prindle[16], F. Pühlhofer[12], J.G. Reid[16], R. Renfordt[10], W. Retyk[15], H.G. Ritter[2], D. Röhrich[10], C. Roland[7], G. Roland[10], A. Rybicki[6], T. Sammer[13], A. Sandoval[7], H. Sann[7], A.Yu. Semenov[9], E. Schäfer[13], R. Schmidt[7], D. Schmischke[10], N. Schmitz[13], P. Seyboth[13], F. Sikler[4], B. Sitar[19], E. Skrzypczak[15], G.T.A. Squier[3], H. Stelzer[7], R. Stock[10],P. Strmen[19], H. Ströbele[10], I. Szarka[19], I. Szentpetery[4], P. Szymański[5,14], J. Sziklai[4], M. Toy[2,11], T.A. Trainor[16], T. Ullrich[17], M. Vassiliou[1], G. Veres[4], G. Vesztergombi[4], D. Vranic[5,18], F. Wang[2], D.D. Weerasundara[16], S. Wenig[5], C. Whitten[11], N. Xu[2], T.A. Yates[3], J. Zimanyi[4], X.-Z. Zhu[16]

[1]Department of Physics, University of Athens, Athens, Greece, [2]Lawrence Berkeley National Laboratory, University of California, Berkeley, USA, [3]Birmingham University, Birmingham, England, [4]KFKI Research Institute for Particle and Nuclear Physics, Budapest, Hungary, [5]CERN, Geneva, Switzerland, [6]Institute of Nuclear Physics, Cracow, Poland, [7]Gesellschaft für Schwerionenforschung (GSI), Darmstadt, Germany, [8]University of California at Davis, Davis, USA, [9]Joint Institute for Nuclear Research, Dubna, Russia, [10]Fachbereich Physik der Universität, Frankfurt, Germany, [11]University of California at Los Angeles, Los Angeles, USA, [12]Fachbereich Physik der Universität, Marburg, Germany, [13]Max-Planck-Institut für Physik, Munich, Germany, [14]Institute for Nuclear Studies, Warsaw, Poland, [15]Institute for Experimental Physics, University of Warsaw, Warsaw, Poland, [16]Nuclear Physics Laboratory, University of Washington, Seattle, WA, USA, [17]Yale University, New Haven, CT, USA, [18]Rudjer Boskovic Institute, Zagreb, Croatia. [19]Comenius University, Bratislava, Slovakia [20]University of Houston, Houston, TX, USA

[$]present address: Kent State Univ., Kent, OH, USA
[*] EC fellow

1 Introduction

The NA49 experiment was constructed to search for the predicted phase transition from hadrons to deconfined quarks and gluons in Pb+Pb collisions at the SPS. Such reactions provide the largest most energy dense collision system for controlled study in the laboratory. NA49 was optimized to study hadronic observables in strong interactions of nucleons and nuclei, with a specific aim at large acceptance coverage for momentum reconstruction as well as for particle identification of most produced particles. With its large phase space coverage NA49 is able to measure global properties of individual events in Pb+Pb collisions.

The first round of experiments with heavy ions at CERN, and especially the recent Pb+Pb collisions, have produced an impressive and varied quantity of data. The interpretation of these results is still subject of vivid discussion and even controversy [1, 2]. The most far reaching hypothesis claims the production of a Quark Gluon Plasma (QGP) in heavy ion collisions at the SPS. In consequence to this situation, the NA49 collaboration intends to extend its own contributions [3, 4, 5, 6] in a long–term research programme with the attempt to answer several essential questions such as:

- To what extent is thermal and chemical equilibrium reached in nucleus–nucleus collisions?
- What is the nature of the hadronization mechanism?
- What is the mechanism of baryon number and energy stopping in high energy hadron collisions?
- Does a transformation from confined to deconfined matter occur and at which energy does it happen?

The NA49 programme is complementary to experiments which investigate properties of dense matter by measurement of probes like J/ψ and dileptons. It has become quite evident that the interpretation of these results requires a comprehensive knowledge of the environment in which such signals are produced. NA49 is ideally suited to provide this information.

In its initial phase, the NA49 collaboration has been concentrating on an exploratory investigation of central Pb+Pb interactions at the highest SPS energy. After it had been demonstrated in 1994, with part of the detector set-up, that the ambitious detector programme of precision tracking and identification up to very high track densities could be successfully achieved, two complete heavy ion running periods have been dedicated to this aim in 1995 and 1996.

These initial data taking campaigns have yielded about 1.5 million central Pb+Pb events. The analysis of this vast data sample is in itself a considerable challenge which has required the development of a large hardware and software infrastructure and which is still being actively pursued.

The analysis makes use of the unique capability of the NA49 detector to combine the study of particle yields with correlation analysis and physics on the event–by–event level. First results [3, 4, 5, 6] shed new light on the salient questions concerned with the behaviour of matter at large energy density. In particular they show that the step from collisions of medium-size nuclei (as they have been available in the past) to large–size systems does not lead to a substantial change in the observables considered as possible signals of a phase transition like the pion/baryon and strangeness/pion ratios. A significant change in these observables is seen only when comparing nucleon–nucleon interactions with collisions of medium– and large–size nuclei at SPS energy. Our event–by–event analysis of Pb+Pb data does not reveal the appearance of dynamically different new event classes down to the permille level of admixture. These results

together with the energy dependence of pion and strangeness production in nucleus–nucleus (A+A) collisions might indicate that we already passed the threshold energy for the creation of a deconfined partonic state (ideally the QGP) with SPS sulphur beams. This hypothesis is not in contradiction with the NA38/NA50 results concerning anomalous J/Ψ suppression in central Pb+Pb collisions only. This suppression requires energy densities higher by a factor of 2–3 than the critical energy density [7]. Thus we propose to extend the NA49 experimental programme to study heavy ion collisions at lower SPS energies and lower masses of colliding nuclei to find and investigate the QCD transition.

There are, however, effects which show a change with increasing size of the colliding nuclei. Let us mention here the very pronounced change in the inclusive distribution of baryons – as compared to pions – with increasing nuclear size ("stopping") and the steadily increasing transverse activity observed for all hadronic observables.

Interpretation of the observed effects and better understanding of the underlying physics requires more accurate knowledge of the basic collision processes than is available at present. For instance the understanding of baryon number transfer and stopping, the building–up of energy density and the corresponding level density including spin states, needs to be improved. It has to be questioned to which extent the statistical approach, which provides a welcome guideline with simple global variables through the complicated microscopic world of soft QCD phenomena, can be maintained. We feel that a serious and continued experimental effort is necessary in order to improve the situation. This effort has certainly to include the "microscopic" collision environments given by proton(pion)–proton (p(π)+p) and proton(pion)–nucleus (p(π)+A) interactions [8]. It also has to open up the parameter space by varying both the nucleus mass and projectile energy.

We feel that the NA49 experiment is ideally suited to these tasks. NA49 is for the time being the only large acceptance tracking facility offering particle identification over most of the acceptance and up to the highest particle densities at SPS energies.

By adding a liquid hydrogen target to the experimental setup, we have obtained in a 1996 pilot run a sample of about 1 million p+p events which we are analyzing at the moment. In 1997 we have obtained an event sample of similar size in p+A and π+A collisions, using Al and Pb targets at two beam energies. We added a centrality trigger detector to the setup in order to be able to measure and select on impact parameter. This should be of prime importance for the detailed comparison with central Pb+Pb collisions.

In the course of the future programme of NA49, several more additions to the original detector setup are foreseen in order to enhance its physics potential:

- Pestov TOF (PesTOF) counter arrays inside the first vertex magnet to enhance particle identification in the backward rapidity hemisphere,
- a forward TPC detector extending the acceptance from particle momenta of 80 GeV/c to the kinematic limit for a study of the leading hadrons,
- Si drift chamber microvertex detectors for improved spectroscopy of short lived particles, in particular, to attempt the measurement of D meson production.

The anticipated detector additions serve at the same time as tests for detector developments for the ALICE experiment at the LHC. This synergy is essential for the proper evaluation of detector performance in the correct range of experimental conditions (e.g. track density and overall detector load) to be expected at LHC.

This report is organised as follows: Section 2 contains an overview of the NA49 experimental setup and detector performance. Section 3 gives a summary of the NA49 experimental results on Pb+Pb, p+p and p+A collisions and their implications for the future programme of NA49. Section 4 discusses the future plans and requests.

2 Detector Layout and Performance

2.1 Experimental Setup and Acceptance

The experimental setup of NA49 is shown in Fig. 1. It comprises four Time Projection Chambers for tracking and energy loss measurement, four Time–of–Flight walls and an array of PesTOF counters for additional particle identification, calorimetry for neutral particle detection and triggering, and a system of beam detectors.

Two medium size TPC's (VTPC–1/2) of 3 m^3 gas volume each, are located inside the Vertex–Magnets (VTX–1/2) with up to 1.5 T field strengths each. Two large size TPC's (MTPC–L/R) of 20 m^3 gas volume each, are positioned downstream of the magnets for high–precision dE/dx measurement and acceptance coverage in the forward direction. The TPCs are read out by a total of 182 000 electronics channels which use highly integrated custom designed chips [9].

The Time–of–Flight scintillator systems complement particle identification in the region near minimum ionization and for tracks with insufficient length for precise dE/dx determination.

A Ring Calorimeter (RCAL) offers photon and neutral particle measurement as well as transverse energy determination over full azimuth. A Veto Calorimeter (VCAL) covering the extreme forward direction is used for triggering on central events in Pb+Pb interactions.

A flexible system of beam detectors and target stations is used for the different running conditions.

Position and direction of each beam particle is measured by a system of proportional chambers with cathode readout (BPD–1/2/3). A minimum set of scintillation counters (for proton and pion beams) or very thin Cherenkov detectors (for heavy ion beams) allows beam definition and triggering (S1–S4).

Metal foil targets are used for Pb+Pb and p+A running (Fig. 1a and c). A liquid hydrogen target is available for p+p running (Fig. 1b).

The acceptance coverage amounts to about 80 % of all charged particles. The acceptance losses are concentrated around the up–down regions in azimuth (due to the horizontal separation of the TPC system with respect to the beam imposed by the Pb beam running) and in the backward rapidity region below –1 unit in the cms. This is illustrated in Fig. 2 where rapidity distributions for pions are shown, in transverse momentum bins, for produced and accepted particles in p+p events at 158 GeV/c beam momentum. For central Pb+Pb interactions this means that out of about 1500 produced charged particles 1200 are detected.

2.2 Tracking Performance

The set of Time Projection Chambers measures up to 234 space points on tracks of up to 13 m length. Since no other, independent tracking element (except for the determination of the incoming beam) is available, we have to rely entirely on the geometrical quality and stability of the TPC system alone. The challenging task of global track reconstruction through several independent TPC's necessitates very considerable efforts in reconstruction software, detector controls, understanding of electric and magnetic field distortions, and overall detector geometry.

The detectors are surveyed with optical methods to a precision of about 200 μm over the full extension of the experiment. This precision can be verified using single high momentum muon tracks traversing the complete detector. The average residuals with respect to a straight line fit, shown in Fig. 3a, reconstructed using only the survey geometry, demonstrate that (i) the overall alignment is indeed of this precision and (ii) the additional distortions introduced by imaging imperfections inside the TPC's are small. After application of small corrections to the detector alignment an overall residual spread of less than 100 μm can be achieved (Fig. 3b). The corresponding precision of vertex reconstruction is of order 150 μm in the plane transverse

to the beam, as shown in Fig. 4.

In the case of high track densities there are many tracks which are very close to each other over the complete length of a TPC. For illustration in Fig. 5 the top view of a single Pb+Pb event is shown in a small wedge around the mid plane of the detector. Therefore one has to define a mean track pair distance over the full length of a track. The reconstruction efficiency as function of this mean distance is shown in Fig. 6. It reaches 50 % at a mean track distance of 10 mm reflecting the width of the charge clusters for the employed cool gases in both transverse and longitudinal direction. Cluster unfolding could further improve on this value.

The overall tracking efficiency is above 95 % for p+p and p+A interactions. For central Pb+Pb collisions the efficiency may decrease to about 85 % in the regions of high track density. The momentum resolution can be parametrized as

$$\sigma(p)/p = 10^{-4} \cdot p(GeV) + 1.5 \cdot 10^{-3}. \quad (1)$$

With this performance resonances and secondary decay vertices can be reconstructed even in the high track density environment of central Pb+Pb events, as demonstrated in Fig. 7 for neutral strange particles.

2.3 Particle Identification Performance

Particle identification via energy loss (dE/dx) measurement constitutes a major advantage of the TPC tracking system, as more than 67 % of all reconstructed tracks have sufficient track length for reasonable separation power below and above the minimum of ionization (Fig. 8). Near the minimum, the Time–of–Flight system offers another 6 % of acceptance for identification which is especially efficient when combined with dE/dx.

The dE/dx determination is particularly challenging as most of the track momenta fall into the relativistic rise region and as – due to the high track densities – pad readout only is used for both coordinate and charge measurement. Fig. 9 shows scatter plots of dE/dx against momentum for positive and negative particles in p+p interactions. A dE/dx resolution of better than 4 % is reached for tracks in the MTPC's up to the highest accepted momenta.

This allows for excellent pion–proton separation and even for reasonable enrichment of kaon samples on the track–by–track level, as shown in Fig. 10 for a momentum bin around 10 GeV/c.

The Time–of–Flight systems reach time resolutions of 60–80 ps for arrays of more than 1000 independent counters, see Fig. 11. This results in the combined separation power of the experiment shown in Fig. 12, where the TPC dE/dx information is plotted against TOF mass squared in central Pb+Pb collisions.

A recent addition to the experiment is an array of PesTOF counters installed between the two Vertex magnets, see Fig. 1. These counters are expected to reach inherent time resolutions of less than 50 ps and constitute an extension of TOF coverage into the region of backward rapidities. A first test run with 12 counters has taken place in fall 1997.

3 Physics Results and Implications for the NA49 Programme

A review of physics results of the NA49 Experiment is given together with a brief summary of the current status of the discussed physics framework. Implications for the future programme of the NA49 Experiment are underlined.

3.1 Nucleus–Nucleus Collisions

The fundamental theory of strong interaction, quantum chromodynamics (QCD), predicts a phase transition at high temperature (density). Lattice results [10] for QCD with dynamical

quarks indicate that the transition temperature is about T_C = 140–180 MeV and the corresponding critical energy density is about 1 GeV/fm^3. In this so called Quark Gluon Plasma [11] color charge is screened rather than confined. In contrast to low temperature (density) matter a QGP consists of independent quarks and gluons. The basic feature of the transition from hadronic matter to QGP is an increase of the effective number of degrees of freedom and a reduction of the effective masses of quarks in case of chiral symmetry restoration.

High energy nuclear collisions make it possible to create, in the laboratory, 'macroscopic' space–time domains with high energy density. The volume and the energy density are determined the sizes of the colliding nuclei (geometry) and the collision energy. Nucleus–nucleus collisions are studied at the SPS at the highest presently available energy (200 A·GeV for the S beam and 158 A·GeV for the Pb beam).

The experimental data on total transverse energy production [3] allows to infer that the early stage energy density in central collisions of large nuclei at the SPS is significantly above 1 GeV/fm^3. Thus it is larger than the critical energy density obtained using lattice QCD simulations. It is obvious that at these high energy densities partonic aspects will come into play. It is the goal to show that these partons form, albeit for a short time, a new form of matter, the QGP. Among the proposed signals of the QGP are strangeness enhancement [13], entropy enhancement [14] and J/Ψ suppression [7] and, indeed, they have been observed experimentally [15, 18, 19]. The energy dependence of pion and strangeness production [20] changes between AGS ($\approx$ 15 A·GeV) and SPS ($\approx$ 200 A·GeV) energies.

The observed behaviour is in qualitative agreement with the hypothesis that the transition to Quark Gluon Plasma occurs within this energy range. If so we propose to attempt to locate the onset of this transition at intermediate energies and masses of nuclei.

However, there are still other ways to interpret certain aspects of the data without assuming equilibration and creation of a QGP. This ambiguity in the interpretation is difficult to resolve on the theoretical level due to the phenomenological character of the description of soft QCD processes. The NA49 Experiment is capable, by construction, to provide a comprehensive body of data. This should allow to answer several crucial physics questions already outlined in the introduction and further discussed in this section.

3.1.1 Transition to the Quark Gluon Plasma

A new dimension in the interpretation of the data can be reached by systematic studies of the energy dependence of collision properties. In the energy range in which the transition occurs some observables may change rapidly or reveal a non–monotonic behaviour. The data on A+A collisions at lower energies (AGS: $\approx$15 A·GeV, JINR Dubna: $\approx$4.5 A·GeV, Bevelac LBL and SIS GSI: below 3 A·GeV) together with the existing data at the highest SPS energy suggest a search for these effects in pion and strangeness [21] production at intermediate energies, 30–100 A·GeV. In the following we outline this future research goal by reviewing present experimental results and ideas concerning the signatures of the phase transition.

Pion and Strangeness Production

Most of the entropy created during a high energy nuclear collision is carried away by the produced pions. Thus the increase in the number of degrees of freedom at the early stage of the collision due to a transient QGP phase should be reflected in more abundant pion production. In fact, the energy dependence of the difference between the mean pion multiplicity per participant baryon for central A+A collisions and nucleon–nucleon (N+N) interactions indicate a change (Fig. 13 [20]). Up to the AGS energy the pion production in A+A collisions is suppressed

by about 0.3 pion per baryon relatively to N+N interactions, approximately independent of collision energy and the size of colliding nuclei. This suppression pattern is not continuing at SPS energies. The data on central S+S and Pb+Pb collisions show an enhanced pion production by about one pion per baryon. The transition from suppression to enhancement occurs between AGS and SPS energies.

A reduction of the mass of strangeness carriers during the transition from hadronic matter ($m_K \approx 500$ MeV/c^2) to QGP ($m_S \approx 150$ MeV/c^2) as well as a change in the effective number of strange degrees of freedom should be reflected in the energy dependence of strangeness production. The ratio of the multiplicity of strange particles to pions is shown in Fig. 14 for central A+A collisions and N+N interactions [20]. Both ratios show a rapid increase from Dubna to AGS energies. The ratio for N+N interactions increases further when going from AGS to SPS energy. No such increase is observed for central A+A collisions, indicating a change of the energy dependence of the relative strangeness (to pion) production again occuring between AGS and SPS energies. On a qualitative level this change can be interpreted as follows [20]. Due to the large mass of strange hadrons relative to the temperature in hadronic matter the ratio of strangeness to pions (approximately equal to the ratio of strangeness to entropy) grows rapidly with the temperature (collision energy). A much weaker energy dependence of the strangeness to entropy (pion) ratio is predicted for the QGP phase where the mass of strangeness carriers is similar or smaller than the temperature of matter. Note that this simplified interpretation is based on the assumption that the entropy and the number of strangeness carriers reach equilibrium in the early stage of the collision and are conserved during the system evolution.

As mentioned above the early stage energy density estimated on the basis of transverse energy measurements at the SPS using Bjorken initial conditions [12] is higher than the critical energy density of QGP obtained in lattice QCD calculations. This yields an upper limit for the transition collision energy $E_C < 160$ A·GeV. An estimate of the lower limit of E_C performed using Landau initial conditions yields $E_C > 30$ A·GeV [35]. These estimates of E_C limits based on energy density agree well with the above tentative experimental localization of E_C using pion and strangeness data.

The observed energy dependence of pion and strangeness production together with the detection of Ψ' suppression in S+A and J/Ψ suppression in central Pb+Pb collisions may suggest that at the top SPS energy the matter created in A+A collisions is initially in the deconfined partonic state. Consequently, we should try to locate the collision energy at which the transition occurs and study the transition properties.

Other Signals of Transition

In the following we describe two other signatures of the QCD phase transition which can be measured by the NA49 Experiment near the transition energy.

Close to the transition energy a "softening" of the equation of state (EOS) is expected [35]. In the extreme picture of Landau initial conditions a stationary 'slow–burning fireball' is created. The strong longitudinal and transverse expansion of matter observed at AGS and SPS energies should then be suppressed. Moreover the life time of the fireball should increase significantly [35].

Details of the space–time evolution of the matter created in nuclear collisions is "measured" by the analysis of inclusive spectra and two particle correlations. The large acceptance, high statistics and high momentum resolution of the NA49 experiment allow for an estimation of expansion velocities, overall reaction time and duration of particle emission [5]. We should be able to observe a hypothetical non–monotonic energy dependence of these parameters when

crossing the ”softest” point of the EOS. The longitudinal flow rapidity and the duration of pion emission obtained for central Pb+Pb collisions at 158 A·GeV are shown in Fig. 15 [5] as a function of the pion pair rapidity. In the extreme case of a ‘slow–burning fireball’ the longitudinal flow rapidity should be independent of pion pair rapidity and equal to the rapidity of the fireball (horizontal dotted line in Fig. 15). The duration of particle emission may reach 10–20 fm/c in comparison to the few fm/c measured at 158 A·GeV (see Fig. 15). In the latter case, of central Pb+Pb collisions, the initial energy density is far above the critical QCD energy density (as follows e.g. from the J/Ψ suppression pattern). The system is therefore in the state of rapid expansion once it reaches the hadronization point – thus leading to the short emission duration in this reaction.

In the transition energy range large event–by–event fluctuations (pion multiplicity, strangeness content) may be expected due to fluctuations in the plasma creation processes: nucleation [36] or percolation [37]. Thus characteristic changes in the event–by–event fluctuation pattern should provide an additional signature of the QCD phase transition which can be measured by the NA49 Experiment. We are developing a method, the scaled correlation analysis, which has the potential to detect unusual event classes even below 10^{-3} level [38].

We conclude that the search for the transition to QGP requires a systematic study of basic properties of the A+A collisions as a function of the collision energy. This search should be started from the energy close to the transition energy ($\approx$ 30–80 A·GeV) as in this case unusual behaviour in the space–time evolution of the matter and large event–by–event fluctuations may be expected. Such results at such energy would be more conclusive than those at energies outside the transition region where no such anomalies are expected.

3.1.2 Thermal and Chemical Equilibration and Hadronization

One of the key questions in the interpretation of the data from high energy nuclear collisions is to which extent and at which stage of the collision thermal and chemical equilibration is reached. Only if the created partonic system is close to equilibrium we may be able to search for the QGP – equilibrated matter of deconfined quarks and gluons. Equilibration allows to use thermo– and hydrodynamical models in the data interpretation instead of non–equilibrium parton (hadron) cascade approaches which are limited by our poor knowledge of soft QCD processes.

The NA49 Experiment provides for a unique possibility to study thermal and chemical equilibration in nuclear collisions. This should allow to distinguish between equilibrium and non–equilibrium models and help in understanding properties of soft QCD processes.

Thermal Equilibration

The inverse slope parameters of the transverse mass distribution at SPS energies are typically 150 MeV for p+p interactions and reach 400 MeV for central Pb+Pb collisions at the SPS (Fig. 16) [6]. The strongest increase is observed for heavy hadrons. This effect finds a potential interpretation within hydrodynamical models in which local thermal equilibrium of transversely expanding matter is assumed [22]. Simultaneous measurements of single particle spectra, and of Bose–Einstein correlations between two pions allow to estimate temperature and transverse flow velocity at freeze–out [5] (Fig. 17). However, it has been demonstrated that, at least, the spectra can also be described by initial state scattering models, which do not require the existence of hydrodynamical flow [23] and which attribute the broadening of transverse momentum distributions to multiple scattering of the incident nucleon and its remnants in the target nucleus. The parameters of the initial state scattering models can be fixed by a fit to p+A data, leading

to a description of A+A spectra that is of similar quality as that of the hydrodynamical models. A study of inclusive particle spectra alone is therefore clearly not sufficient to understand whether thermal equilibration was established in the course of the nuclear collision. We note that a comparable study for Bose–Einstein correlations in initial state scattering models has not been carried out yet.

Moreover the occurence of thermal equilibration can be quantified by a study of event–by–event fluctuations [24]. The method is based on the fact that hadrons produced in p+p interactions are correlated in momentum space. This correlation leads to significant event–by–event fluctuations (e.g. in transverse momentum) predicted by superposition models for nuclear collisions [24]. Introduction of initial state scattering further increases these fluctuations [25] in central nucleus–nucleus collisions.

To the contrary, thermal equilibration (occuring possibly at the early stage of the collision) washes out these correlations and consequently leads to a reduction of event–by–event fluctuations. The result of NA49 for central Pb+Pb collisions at the SPS [26] indeed indicates that the particles are emitted in almost uncorrelated way as expected in the case of thermal equilibrum. Fig. 18 shows that the fluctuation measure Φ_{P_T} [24] is close to zero, well below the value expected for superposition models. This finding contradicts [25] the expectations from non–equilibrium initial state scattering models [23] proposed to interpret single particle spectra in nucleus–nucleus collisions at high energy.

It is obvious, however, that for a complete understanding of the thermalization process systematic measurements of the event–by–event fluctuations in p+p and p+A interactions and A+A collisions are needed as a function of the nuclear mass number.

Chemical Equilibration and Hadronization

The relative abundance of the various produced hadrons (the chemical composition of the final state) is very different when we compare p+p interactions and central Pb+Pb collisions at the SPS [6]. The most striking effect is an increase by a factor of about 2 of the relative (to the pion yield) production of (anti)strange hadrons [15, 16] called strangeness enhancement (see Fig. 19). This increase is observed already in central S+S collisions at the SPS. An intuitive explanation of this effect is that for collisions of large enough nuclei the chemical equilibration of strangeness is reached in the QGP, where fast strangeness equilibration is expected [13, 17]. However a significant part of the strangeness enhancement effect can be also explained in non–equilibrium initial state scattering models by an additional production of $s\overline{s}$ pairs from the nucleon sea [28].

The chemical composition of the final state can be further modified by secondary inelastic processes at the hadronic level. Recent analysis of hadron production in e^++e^- and p+p [29] interactions within a hadron gas model suggests that the particle yields resulting from hadronization are governed primarily by phase space. A similar analysis performed for central Pb+Pb collisions at the SPS based on a large number of different hadronic states ($p, \Lambda, \pi^-, K, \phi$ and the antiparticles) measured by the NA49 Experiment [30] (see Fig. 20) finds a similar temperature parameter (the temperature for all analyzed processes is in the range 160–190 MeV). This suggests that the hadronization process imposes common characteristics on all these interactions, and the secondary inelastic processes on the hadronic level play a minor role. The only but very significant difference between elementary processes and central A+A collisions, the increase of the level of strangeness saturation[1)] should be attributed to the prehadronic stage.

[1)] The strangeness saturation factor γ_s [31] increases from about 0.45 for elementary interactions to 0.6–0.7 for central A+A collisions at SPS [30]

Direct verification of chemical equilibration is needed to distinguish between equilibrium and non–equilibrium models. Again, event–by–event fluctuations provide a suitable signature. As a first result we show in Fig. 21 the event–by–event fluctuation of the K/π ratio in central Pb+Pb collisions. It exhibits no significant fluctuations beyond those given by detector resolution and statistics, thus indicating that the strangeness enhancement effect is present in all central Pb+Pb collisions and that dynamical fluctuations are small.

More sensitive analysis can be done by the study of event–by–event fluctuations of hadronic multiplicities [32], in a way similar to the measurement of thermal equilibration [24]. This kind of analysis, however, requires detailed data on hadron production in p+p interactions in order to establish the correlations in particle production present in elementary processes. An analysis of the data from p+A and A+A collisions will allow then to quantify the approach to chemical equilibration in nuclear collisions.

Hadronization: Spectroscopy of ϕ, Ξ, $\Lambda(1520)$ and D–mesons

The estimation of features of the hadronization and freeze–out processes via hadro–chemical models is severely hampered by a multitude of reconance decay and feeding contributions from higher states into π, K, $\overline{p}$, Λ and $\overline{\Lambda}$ signals. On the contrary, ϕ mesons and $\Lambda(1520)$ hyperons are are likely to be directly produced. Likewise, the Ξ and $\overline{\Xi}$ hyperon family receives feeding only from the rare Ω state. The study of these states will be enhanced by the future PesTOF detector. Distribution of kinematical quantities of these hadrons are therefore more directly coupled to the underlying dynamical processes.

We mention, in closing, a plan to equip the front sector of the NA49 Experiment with a Microvertex Si–drift detector once several prototype planes would become available in the course of ALICE development. This is expected to allow for a measurement of the production rates of D mesons in nuclear collisions.

3.2 Nucleon–Nucleon Interactions

Nucleon-Nucleon interactions constitute one of the basic processes of strong interaction. As such, their understanding will determine to a large extent success or failure of any attempt to master the more complex hadronic systems encountered in p+A and A+A collisions.

Even more than 20 years after the introduction of QCD as the general theoretical framework of hadronic physics, our understanding of this elementary process is still all but satisfactory, at least in the nonperturbative sector which comprises the vast majority of the observed cross sections.

This problem is only partially imputable to the theoretical difficulties in handling soft hadronic phenomena. It is above all the absence of dedicated detectors and therefore the lack of precise, consistent and selective experimental data sets which precludes stringent tests of the abundance of different theoretical approaches.

Up to now most data are only available on the level of single inclusive cross sections and even here the situation is neither characterized by completeness nor by satisfactory internal consistency. This situation is reflected in the large number of phenomenological models all tailored to describe the available data to their degree of precision, without offering real selectivity nor predictivity for more involved observables.

Any real progress in the field has to come from precise experimental data which are able to scrutinize the deeper layers of elementary hadronic collisions. Further toward this aim one should measure correlations of identified particles over most of the available phase space, from the semi–inclusive level up to exclusive states. This means apparatus with wide acceptance cov-

erage and simultaneous particle identification capabilities for most of the produced secondaries.

Exactly this performance can be offered by the NA49 experiment. A look at the acceptance plots (Fig. 2) and dE/dx performance (Fig. 8, 9 and 10) quoted above shows that both requests can be fulfilled for the full projectile hemisphere and down to well below central rapidity.

We have started an exploratory study of these possibilities using a small fraction of the available statistics from our proton–proton run in 1996. As an example from the vast field of unexplored non–perturbative phenomena we will address here the question of baryon number transfer ("stopping") as it has direct relevance to one of the more pronounced phenomena in heavy ion collisions.

3.2.1 The Problem of Baryon Number Transfer

One of the most striking features of inclusive particle production in p+p collisions is the fact that the invariant proton distribution increases approximately linearly [39] with Feynman x_F (with the exception of the diffractive peak) whereas the pion distributions show a strong decrease as function of x_F reflecting the longitudinal structure functions of the corresponding valence quarks in the proton. This is recalled in Fig. 22 where we show x_F distributions for charged pions measured in our experiment. The steeper longitudinal momentum dependence for negative pions produces the well–known [40] strong increase of the π^+/π^- ratio with x_F shown in Fig. 23.

This apparent reflection of parton structure in pion production is not as easily interpretable for baryons: which processes lead to the broad longitudinal distributions that are approximately flat in baryon number? Does one see a real energy loss of the incoming proton ("stopping") or does one have to do with a transfer of baryon number? How does this transfer operate? How does it lead to overall baryon number conservation?

Considerable theoretical interest [43] has been raised recently concerning this subject, mostly induced by the difficulties to predict and understand heavy ion collisions. In order to obtain a deeper insight, correlation measurements are indispensible. To conduct those measurements it is mandatory to exclude the region of low x_F (where baryon–antibaryon pair production gives a strong contribution) as well as the region of high x_F (where diffractive processes prevail).

Events with protons in the x_F interval 0.2–0.5 have therefore been selected to obtain a sample of semi–inclusive pion distributions. A comparison to events from π^+ beams would further clarify the underlying mechanism, as the effects of single valence quarks would be eliminated.

3.2.2 Charge and Momentum Correlations between Baryons and Mesons

Comparing the invariant pion cross section obtained with the above proton selection (Fig. 24) with the unconstrained data set of Fig. 22 we observe a distinct correlation pattern.

- The cross section for negative pions becomes about equal to the one of positive pions such that the charge ratio is close to unity over the measured x_F range.
- The shape of the proton–selected and unselected pion x_F distributions is not much different up to about $x_F \approx 0.5$ where energy conservation starts to cut into the selected distribution. As the protons take a considerable fraction of beam momentum, $\langle x_F(\text{proton})\rangle \approx 0.35$, this means that the relative share of the remaining longitudinal momentum carried by pions is higher in the proton selected sample.

– This modified energy sharing can be brought out more clearly by redefining x_F (on an event–by–event basis) as

$$x'_F = \frac{x_F}{1 - x_F(\text{proton})}. \quad (2)$$

The so defined x'_F distribution is shown in Fig. 25. Its shape can be described by

$$x'_F \frac{dn}{dx'_F} \approx (1 - x'_F)^2 \quad (3)$$

for both pion charges. In a parton picture this could be interpreted as energy sharing by a quark pair after baryon number transfer, as opposed to the three quark system of the incoming proton.

The clear observation of long–range correlations both in charge and in momentum between protons and pions should allow for increased selectivity in the confrontation of the different theoretical models for baryon stopping. This first simple example demonstrates at the same time the usefulness of correlation studies with identified secondaries already at the first level below the standard inclusive distributions.

3.2.3 Multiplicity Correlations

The large acceptance of NA49 allows a meaningful inspection of multiplicity correlations even without detailed corrections. An example is given in Fig. 26 where the charge multiplicity distribution of unselected p+p events is compared to the one for the proton selection discussed above, $0.2 < x_F(\text{proton}) < 0.5$. We observe that

– the mean multiplicity increases only by about 0.5 units and
– this increase is mainly due to a loss of events in the low multiplicity range, $n_{ch} < 5$. The shapes of the distributions for $n_{ch} > 6$ are quite similar.

This finding is consistent with an event selection excluding low mass diffraction rather than increased particle production for events with ”stopped” protons.

3.2.4 Isobar Spectroscopy

In addition to charge,momentum and multiplicity correlations we can also study the spectroscopy of baryons [41] with higher spin and isospin levels, especially in conjunction with baryon stopping. A strong Δ^{++} signal is in fact correlated with protons in the selection range $0.2 < x_F(\text{proton}) < 0.5$ discussed above. This signal is shown in Fig. 27 in comparison to a relativistic Breit–Wigner mass distribution. Indeed about 30 % of all protons in this range of longitudinal momentum come from the decay of this resonance alone, indicating that probably only a small fraction of all protons can be considered to be produced ”directly”. By combining proton–π^+ mass combinations in the Δ^{++} mass range with a further, negative pion we have access to heavy, singly charged isobars. Our ongoing study indicates that also a considerable fraction of Δ^{++} resonances cascades down from heavier states. A detailed inspection of isobar production rates, especially of different charge states and also including strange baryons, should enable us to establish further constraints on the mechanism behind baryon number transfer.

3.3 Hadron–Nucleus Interactions

The study of hadron–nucleus interactions constitutes a very important intermediate step between elementary hadron-hadron physics and the macroscopic realm of heavy ion collisions. Suffering of course on the one hand from our imperfect understanding of the elementary processes in QCD, this field presents on the other hand our only direct access to a number of essential investigations concerning production and propagation of partons and hadrons in dense nuclear matter.

In this context the depth of nuclear matter traversed by the projectile is a key parameter, in particular it provides a time–scale for the hadronization process. This path length can vary from very peripheral collisions which approximately correspond to hadron–nucleon interactions to very central collisions seeing the full diameter of the nucleus. Hence the drawback of purely inclusive measurements having no knowledge of the collision geometry.

Experimentally one can get a handle on this parameter by determining the number of intermediate energy protons (”grey” protons) ejected from the target by the projectile. This measurement was up to now the realm of comparatively low-statistics bubble chamber experiments with internal targets [42] or of emulsion exposures.

In preparation of the hadron–nucleus experimental programme for NA49, we have constructed a centrality detector which is able to measure and trigger on the number of produced ”grey” protons.

3.3.1 Centrality Detector

The detector has the shape of a vertical cylinder with 16 cm diameter and 20 cm length surrounding a thin ($\approx$ 0.3 % interaction length) foil target. It is a gas detector consisting of 32 proportional tubes read out on 256 cathode elements each covering about 20 msterad solid angle. The counter subtends lab polar angles from of 45 to 315 degrees, leaving free the tracking acceptance wedge of the NA49 spectrometer.

Protons below 150 MeV/c momentum are cut off by range in a copper foil between the target and proportional tubes, thus eliminating evaporation (”black”) protons and fragments. Detection of protons above about 600 MeV/c momentum and pions is suppressed by placing the detection threshold at about three times the most probable energy loss of minimum ionizing particles.

The hit pattern is recorded in latches after threshold discrimination. On–line triggering on the number of produced hits is available via a fast majority coincidence. A typical number distribution of hit cells in untriggered events is shown in Fig. 28 for p+Pb collisions at 158 GeV/c. We have taken data triggered by more than typically 2 and 7 hits in order to obtain high statistics samples also in the tail of this distribution.

The acceptance and performance of the counter has been checked against events from the VENUS generator which contains a reasonable description of the available data on grey protons. This results in the comparison of observed and generated angular distributions presented in Fig. 29. The study allows us to estimate the total acceptance of the counter to be about 40 % of produced grey protons.

3.3.2 First Results on Long Range Correlations

In a five week running period in October/November 1997 we took first exploratory data samples with proton and pion beams, Pb and Al targets, at two beam energies. Typical sample sizes are 10^4–10^5 events. First results including dE/dx identification have become available.

We will concentrate here on a demonstration of long–range correlations between secondary particles in the projectile hemisphere and ”grey” protons from the target nucleus measured by the centrality detector.

Results are presented in the form of cross section ratios from p+Pb and p+p events. This eliminates to first order possible acceptance effects. Fig. 30 shows this ratio for identified protons as function of x_F. The distribution is presented for unselected ”minimum bias” events (Fig. 30a) as well as for events in three different windows in the number of grey protons. Evidently, the baryon number distribution is different in p+Pb collisions as compared to p+p events, and

evidently there is a strong long–range correlation with the number of ejected target protons. Investigations of this type should lead to a better understanding of the problem of baryon number transfer already discussed in the context of p+p interactions.

A similar study is presented in Fig. 31 for identified negative pions. Again a distinct correlation pattern with grey proton production emerges. With our full statistics available we should be able to show whether a limiting shape of the x_F distribution is reached and to which extent longitudinal energy loss of the projectile is responsible for part of the phenomenon. This is topic closely related to jet quenching in A+A collisions at very high energies. Dependences on target size, projectile type and beam energy are evidently important to measure and exploit.

4 Plans and Beam Requests

4.1 Physics Programme

The discussions in Sections 2 and 3 demonstrate that the NA49 detector facility is well suited for coherent and versatile studies of general hadronic observables in nucleus–nucleus collisions as well as proton(meson)–proton and proton(meson)–nucleus interactions. Data sets for this variety of processes, obtained with the same detector setup, will represent a rich sample for a comparison, detailed studies and feedback for theoretical models of "soft QCD" processes, especially as NA49 constitutes at present the only detector facility with wide acceptance and particle identification capability in the SPS energy range. These data sets should allow for a comprehensive search and study of the possible QCD phase transition discussed above.

Given the present status of the field, the physics results obtained by NA49 and discussed in Sect.3, and the already fixed beam schedule for 1998, our future plans are as follows:

- obtain more statistics for Pb+Pb collisions at 158 A·GeV as needed for rarer processes requiring clean TOF identification, such as ϕ, $\Lambda(1520)$ production and KK, pp interferometry,
- study Pb+Pb collisions at lower beam energies in order to establish collision energy dependence of the QGP signals and potentialy locate the QGP phase transition,
- study collisions of lighter ions to investigate how properties of the matter depend on the size of the colliding objects (the level of equilibration, creation of the QGP),
- continue the investigation of proton(meson)–nucleon and nucleus reactions with sufficient statistics as reference for nucleus–nucleus collisions and for a study of soft hadronic phenomena in a simpler environment.

Specific beam time requests for the next years are given below in the section on running plans.

By conception the NA49 detector aims at full coverage of the bulk of hadronic cross sections. As a consequence our rejection factors do in general not exceed about 10^3 at trigger level. Large data samples of order 10^6 events are therefore required in order to keep full flexibility on off line selection of specific event classes. This flexibility to access the deeper layers of soft hadronic phenomena beyond merely inclusive investigation is in our view the biggest asset of the proposed programme.

We concentrate specifically on the following lines of research:

- inclusive measurements: study of inclusive distributions of mesons and baryons including the available range of different flavors, particle ratios and their dependence on kinematical variables,
- study of transverse activity manifest in p_T spectra and in hadron interferometry,
- correlation measurements: charge, momentum and flavor correlation studies with specific interest in long-range correlations between baryons and mesons; general hadron interferometry,

– hadronic fluctuations: study of event–by–event fluctuations concerning multiplicity, kinematical variables and flavor content,
– hadron spectrosopy: study of a wide range of baryon and meson resonances with a special aim at cascading and ”feeddown” as well as spin composition in the different regions of phase space.

A further enhancement of our experimental possibilities can be expected from several detector improvements foreseen in the immediate future and on a longer time scale. These are directly connected with existing detector developments already under way for the ALICE experiment, as discussed in the following section.

4.2 Detector Upgrades and Connection to ALICE Detector Development

The density of particles produced in central Pb+Pb collisions at the LHC, which will have to be dealt with by the ALICE detectors, is by far the highest encountered by any High Energy Experiment performed so far. Understanding and minimizing effects of non-linearities, cross-talk, baseline shifts and saturation in the ALICE detectors and their readout electronics in this environment is crucial for the success of the Experiment.

The only place where conditions approach those that will be found at the LHC, and where these effects can be studied before the final ALICE detectors are built and commissioned, is in central Pb+Pb collisions at the SPS. There is no better way to optimise the performance of the ALICE detectors than to include prototypes in a running experiment with physics goals in the SPS heavy–ion program.

Several additions to the present detector layout are foreseen which make use of detector development programs of ALICE and enhance the physics potential of NA49:

– PesTOF counter arrays inside the vertex magnets for enhanced particle identification in the backward rapidity hemisphere,
– Forward TPC for the study of projectile fragmentation products and for extension of acceptance to the kinematic limit for beam momenta above 90 GeV/c per nucleon,
– Microvertex detectors for extended particle spectroscopy.

Most of the anticipated detector upgrades serve at the same time as a testbed for detector developments in the framework of the ALICE experiment at LHC. It should be stressed that this synergy is essential for the proper evaluation of detector performance in the correct range of experimental boundary conditions (e.g. track density and overall detector load) to be expected at LHC.

4.2.1 PesTOF Time-of-Flight Arrays

Operation and longterm stability of several PesTOF detector units had been extensively tested both at the CERN PS and with cosmic rays at GSI. Stable operation of 9 detectors was maintained over a period of 9 months. A time resolution of 35 ps was found in coincidence studies at CERN. 12 detector units, each with 32 electronic channels (i.e. 384 channels in total), were installed in the NA49 experiment for the p-run 1997 (see Fig. 1). Double threshold discriminators (DTD) of a novel design were tested for the first time in a data production environment. The remaining part of the electronics consisted of custom made QDC’s and standard TDCs. The optimisation of detector performance in terms of stability, electronic channel cross talk, pile up and timing resolution was successfully investigated.

Secondly, the position of the detector modules was selected in order to extend the particle identification capabilities of the NA49 setup, in the case of Pb+Pb collisions, for charged kaons in view of increasing the number of identified kaons per event and extending the acceptance for kaons into the rapidity interval $1.2 < y < 2.2$. The latter improvement is essential for the

determination of the complete rapidity distribution and thus 4π multiplicity of K^+ and K^- mesons. A possible byproduct is the detection of additional ϕ mesons through their decay into K^+/K^-. The regions in phase space of K and ϕ–mesons newly accessible by means of the PesTOF detectors comprise $1.2 < y < 2.2$ for transverse momenta up to 1.3 GeV/c.

In a second step a total of 88 counters (2816 readout channels) will be made available to NA49 for the run in 1998. It is planned to employ custom made TDC ASIC's in this run. It should be noted that the configuration both in terms of the detector setup (the counters are located in a magnetic field at 3.5 m distance from the interaction point behind a TPC) and layout of the frontend readout is of ALICE–type and constitues therefore a first approach to conditions expected for collider runs.

The responsibility for construction and financing of the PesTOF project is carried by GSI and Marburg University. KFKI Budapest are contributing to the DAQ aspects.

4.2.2 Forward TPC

A small Time Projection Chamber will be placed in front of the Main TPC's of NA49 behind the vertex magnets, centered on the beam line (see Fig. 1). This Forward TPC (F–TPC) will cover the range of longitudinal momenta above about 90 GeV/c, thus complementing the acceptance of the standard NA49 detectors up to the kinematic limit. The F–TPC will have 40 cm vertical drift length (corresponding to a transverse momentum coverage of 2 GeV/c) and a readout chamber of dimension 30x40 cm^2. The study of nuclear fragments in the projectile frame will also be possible.

For NA49, the ability to study the longitudinal and transverse momentum spectra of leading mesons and baryons as well as spectator particles in conditions of controlled centrality and in correlation with more centrally produced identified hadrons, will help to expand the physics programme.

According to the high track densities and extended energy loss range to be expected, this F–TPC serves at the same time as prototype detector for the development of the ALICE barrel TPC. Several new features will be included in its design:

- new pad structure (Ring Cathode Chamber, developed in the RD32 project),
- new gating scheme,
- new front end electronics and digitization scheme,
- new electronics mounting technology (TAB),
- new readout chamber construction.

The installation in NA49 will enable a sensitive study of space and two–track resolution as well as dynamic range and occupation density problems in electronics performance.

The long–range operational stability in terms of wire aging and induced self–stable discharges will also be clarified. These latter aspects are of major concern in the ALICE environment.

The CERN, Comenius University Bratislava, and Lund University groups will construct the TPC. The electronics responsibilities will be shared by CERN–NA49, CERN–ALICE, GSI–ALICE and LUND University.

4.2.3 Microvertex Detector

Testing the behaviour of parts of the Inner Tracking System (ITS) of ALICE in a situation where thousand charged particles traverse them will give an increased confidence on their operation at the LHC. Therefore we are investigating the proposal to build a microvertex detector between the target and VTPC-1 of the NA49 setup. This will allow to test them as well as to

develop the analysis software that matches tracks in the TPCs and the microvertex detector well in advance of 2005.

A possible realization in the framework of the ALICE detector development of Si drift chambers in collaboration with the Torino group is under investigation.

4.3 Running Plans

The proposed physics programme of the NA49 Collaboration leads us to the following running plans and beam time requests.

4.3.1 1998 Data Taking Period

The goal of the period is to continue data collection for p+p interactions and Pb+Pb collisions at 158 A·GeV and take test data for a 40 A·GeV run in 1999.

p–beam

NA49 is scheduled for 31 days of proton beam. During this time we plan to increase statistics of p+p data at 158 GeV. The data will be taken with a new, longer hydrogen target which is now under construction. It will improve the efficiency of selection of p+p interactions and reduce possible contamination of background events.

In addition we plan to take first data on p+p interactions at 40 GeV as a test sample for the 1999 data taking period.

ion–beam

The NA49 running time with the Pb–beam at 158 A·GeV is scheduled to be 51 days. For this running period the PesTOF detector and the Forward TPC detector are expected to be completed and will be subsequently commissioned and integrated into the experiment. We plan to take data on minimum bias and central Pb+Pb collisions with these detectors included in the NA49 setup.

A crucial point for the NA49 physics programme is the possibility to obtain a pilot 40 A·GeV Pb–beam. This beam should allow to take first data on central Pb+Pb collisions at a low SPS energy. They are needed for optimization of the NA49 setup with respect to the selected magnetic field and target position configuration before a requested 1999 low energy ion run. After a sucessfull machine development scheduled at the end of the Pb–beam time we are looking forward to the extraction of a 40 A·GeV Pb–beam to the NA49 Experiment (H2 beam line) to give us some useful time for data taking.

4.3.2 1999 Data Taking Period

Our goal for this period is to take data at low SPS energies.

p–beam

For p+p and p+A running beyond 1998 we want to reserve some freedom of choice. In fact our experimental possibilities are by far exceeding the expected available beam time per year. Consequently we will have to adjust carefully the priorities for data taking following the results from the ongoing physics analysis.

We request 6 weeks of p–beam. Presently we intend to take p+p and p+A data at 40 GeV as well as a first sample of data at 80 GeV for test.

ion–beam

We request 6 weeks of Pb beam at low energies. During this period we propose to take data on central Pb+Pb collisions at 40 A·GeV (4 weeks) and 80 A·GeV (2 weeks).

4.3.3 2000 Data Taking Period

One option is to collect p+p and p+A data at energies between 80 and 250 GeV and take data on A+A collisions at 158 A·GeV for various masses of colliding nuclei.

Alternatively the beam time may be used for the measurement of D–meson production, in case our present studies lead to a definitive upgrade with a Si Microvertex detector.

p–beam

We request 6 weeks of p–beam. During this period we want to take p+p and p+A data at beam energy to be decided.

ion–beam

We request 6 weeks of lighter ion (^{32}S, ^{108}Ag) beams at 158 A·GeV. During this period we want to take data on central S+S (3 weeks) and Ag+Ag (3 weeks) collisions at 158 A·GeV.

4.3.4 Data Taking beyond 2000

The goal is a detailed study of energy and system size dependence in the region of low and intermediate SPS energies and nuclear masses.

The requests for the data taking after year 2000 will depend on the results of the analysis of the data taken in 1999 and 2000 runs.

Table 1

The summary of the beam requests of the NA49 Collaboration for the years 1998–2000. The beam energy given in parenthesis are for test runs.

Year	Beam Particle	Beam Energy (A·GeV) (A·GeV)	Beam Time (days)	Reactions
1998	p	158(40)	31	p+p
1998	Pb	158(40)	51	Pb+Pb
1999	p	40(80)	42	p+p, p+S, p+Ag, p+Pb
1999	Pb	40	28	Pb+Pb
1999	Pb	80	14	Pb+Pb
2000	p	80–250	42	p+p, p+S, p+Ag, p+Pb
2000	S	158	14	S+S
2000	Ag	158	14	Ag+Ag

References

[1] Proceedings of the Twelfth International Conference on Ultra–Relativistic Nucleus–Nucleus Collisions, Heidelberg, Germany, May 1996, Nucl. Phys. bf A610 (1996).

[2] Proceedings of the Thirteen International Conference on Ultra–Relativistic Nucleus–Nucleus Collisions, Tsukuba, Japan, December 1997, to be published in Nucl. Phys. bf A (1998).

[3] T. Alber et al. (NA49 Collab.), Phys. Rev. Lett. **75** (1995) 3814.

[4] H. Appelshäuser et al. (NA49 Collab.), nucl–ex/9711001, submitted to Phys. Rev. Lett.

[5] H. Appelshäuser et al. (NA49 Collab.), Frankfurt University Preprint IKF–HENPG/6–97 and hep–ex/9711024, to be published in Z. Phys. **C**.

[6] G. Roland et al. (NA49 Collab.), Quark Matter 97, to be published in Nucl. Phys. **A**.

[7] T. Matsui and H. Satz, Phys. Lett. **178B** (1986) 416.

[8] Y. Pang, talk at QM97 and theoretical discussions at the conference.

[9] F. Bieser et al. (NA49 Collab.), Nucl. Instr. and Meth. **A385 (1997) 535**.

[10] for a review see F. Karsch, Nucl. Phys. **A590** (1995) 367c.

[11] J. C. Collins and M. J. Perry, Phys. Rev. Lett. **34** (1975) 151 and E. V. Shuryak, Phys. Rep. **C61** (1980) 71 and **C115** (1984) 151.

[12] J. D. Bjorken, Phys. Rev. **D27** (1983) 140.

[13] P. Koch, B. Müller and J. Rafelski, Phys. Rep. **142** (1986) 321.

[14] L. Van Hove, Phys. Lett. **B118** (1982) 138.

[15] M. Gaździcki et al. (NA35 Collab.), Nucl. Phys. **A498** (1989) 375c.

[16] S. Abatzis et al. (WA85 Collab.), Heavy Ion Physics **4** (1996) 79.

[17] J. Kapusta and A. Mekjan, Phys. Rev. **D33** (1986) 1304.

[18] M. Gaździcki et al. (NA35 and NA49 Collab.), Nucl. Phys. **A590** (1995) 197c.

[19] A. Bussiere et al. (NA38 Collab.), Z. Phys. **C38** (1988) 117 and M. Gonin et al. (NA50 Collab.), Nucl. Phys. **A610** (1996) 452c.

[20] M. Gaździcki and D. Röhrich, Z. Phys. **C65** (1995) 215 and Z. Phys. **C71** (1996) 55.

[21] M. Gaździcki, Z. Phys. **C66** (1995) 659 and J. Phys. **G23** (1997) 1881 (nucl–th/9706036).

[22] K. S. Lee, U. Heinz, E. Schnedermann, Z. Phys. **C48** (1990) 525.

[23] A. Leonidov, M. Nardi, H. Satz, Z. Phys. **C74** (1997) 535 and S. Jeon, J. Kapusta, Phys. Rev. **C56** (1997) 468.

[24] M. Gaździcki, St. Mrówczyński, Z. Phys. **C54** (1992) 127.

[25] M. Gaździcki, A. Leonidov, G. Roland, hep–ph/9711422.

[26] G. Roland et al. (NA49 Collab.), Proceedings of the Hirschegg Workshop on QCD Phase Transitions, 1997 page 309 and Proc. QM97, Tsukuba, to apear in Nucl. Phys. **A**.

[27] C. Bormann et al. (NA49 Collab.), Proc. of International Symposium ‘Strangeness in Quark Matter 1997’, Santorini (Greece) April 14–18, 1997, to be published in *J. Phys. G*.

[28] A. Capella et al., Z. Phys. **C70** (1996) 507.

[29] F. Becattini, Z. Phys. **C69** (1996) 485 and F. Becattini, U. Heinz, Z. Phys. **C76** (1997) 269 (hep–ph/9702274).

[30] F. Becattini, M. Gaździcki, J. Sollfrank, hep–ph/9710529, to be published in Z. Phys. **C**.

[31] J. Rafelski, Phys. Lett. **262B** (1991) 333.

[32] M. Gaździcki, Frankfurt University Report IKF–HENPG/7–97 and nucl–th/9712050.

[33] E. Fermi, Prog. Theor. Phys. **5** (1950) 570.

[34] L. D. Landau: Izv. Akad. Nauk SSSR, Ser. Fiz. **17** (1953) 51.

[35] C.M. Hung and E. Shuryak, Phys. Rev. Lett. **75** (1995) 4003.

[36] J. Kapusta and A. Vischer, Phys. Rev. **C52** (1995) 2732.
[37] K. Werner, Phys. Rev. Lett. **73** (1994) 1594 and Nucl. Phys. **A572** (1994) 141.
[38] D. Weerasundara et al. (NA49 Collab.), Thirteen International Conference on Ultra–Relativistic Nucleus–Nucleus Collisions, Tsukuba, Japan, December 1997.
[39] V. Blobel et al., Nucl. Phys. **B69** (1974) 454.
[40] J. Singh et al., Nucl. Phys. **B140** (1978) 189,
J. L. Bailly et al., Z. Phys. **C31** (1986) 367,
J. L. Bailly et al., Z. Phys. **C35** (1987) 295.
[41] A. Breakstone et al., Z. Phys. **C21** (1984) 321.
[42] J. L. Bailly et al., Z. Phys. **C35** (1987) 301,
J. J. Whitmore et al., Z. Phys. **C62** (1994) 199.
[43] D. Kharzeev, Phys. Lett. **B378** (1996) 238,
A. Capella, B. Z. Kopeliovich, MPIH-V07-1996 (preprint).

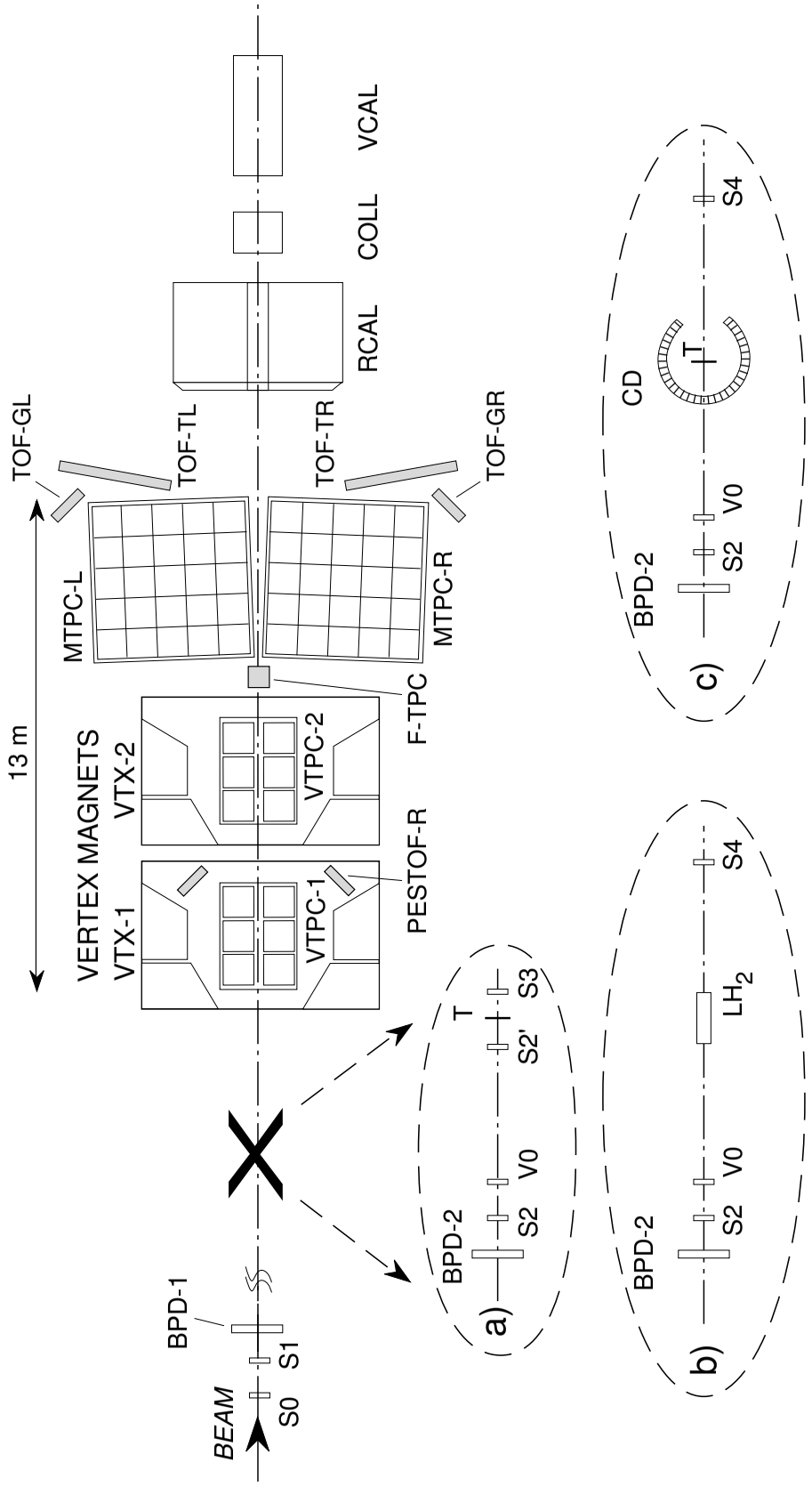

Figure 1: Set–up of NA49 experiment with different target arrangements for a) Pb+Pb, b) p+p and c) p+A collisions. The target position is at the front face of the first Vertex Magnet (VTX–1).

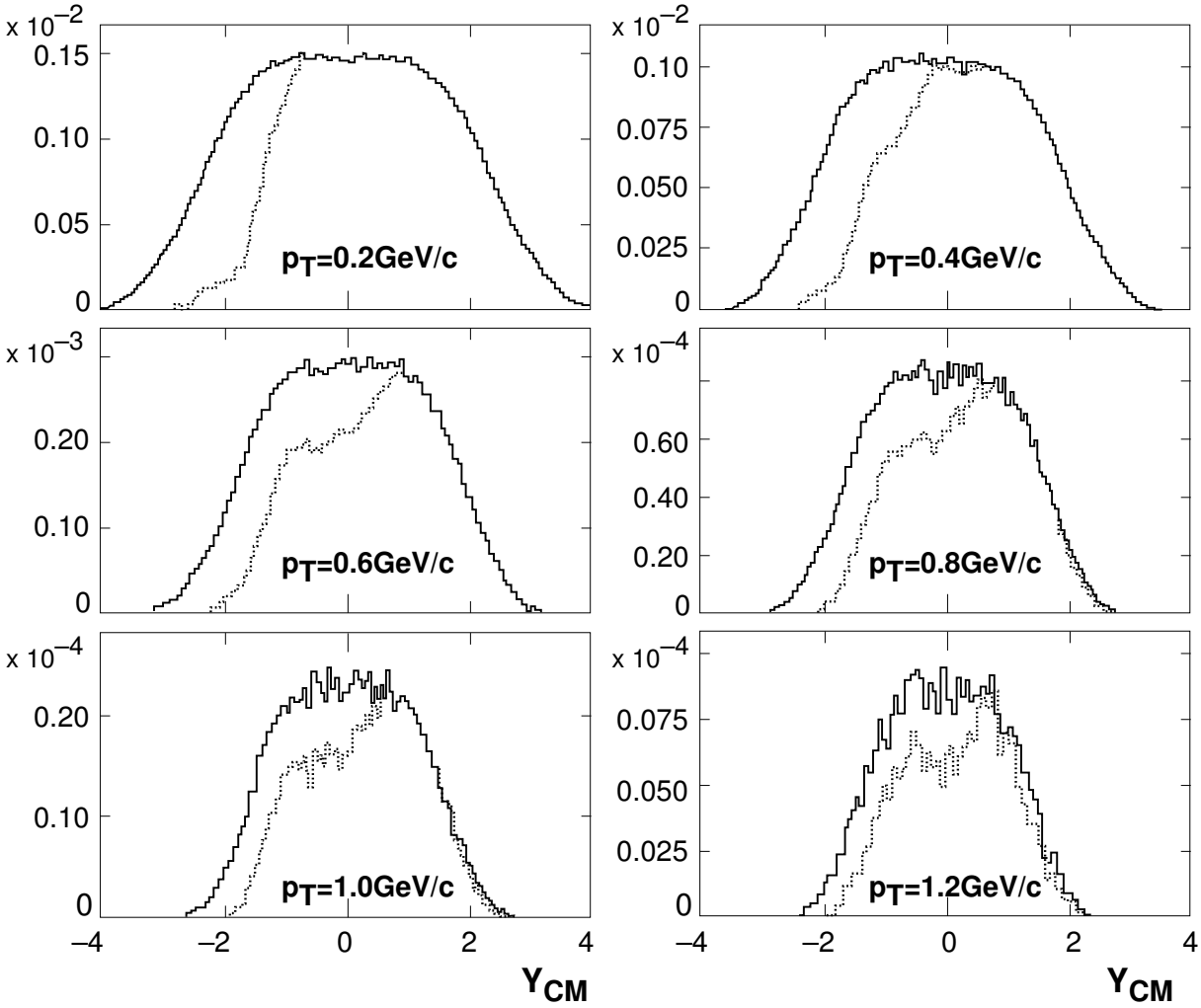

Figure 2: Rapidity distribution of negative pions produced in p+p collisions at 158 GeV/c for different bins in transverse momentum. The full line represents generated particles, the hatched line accepted particles.

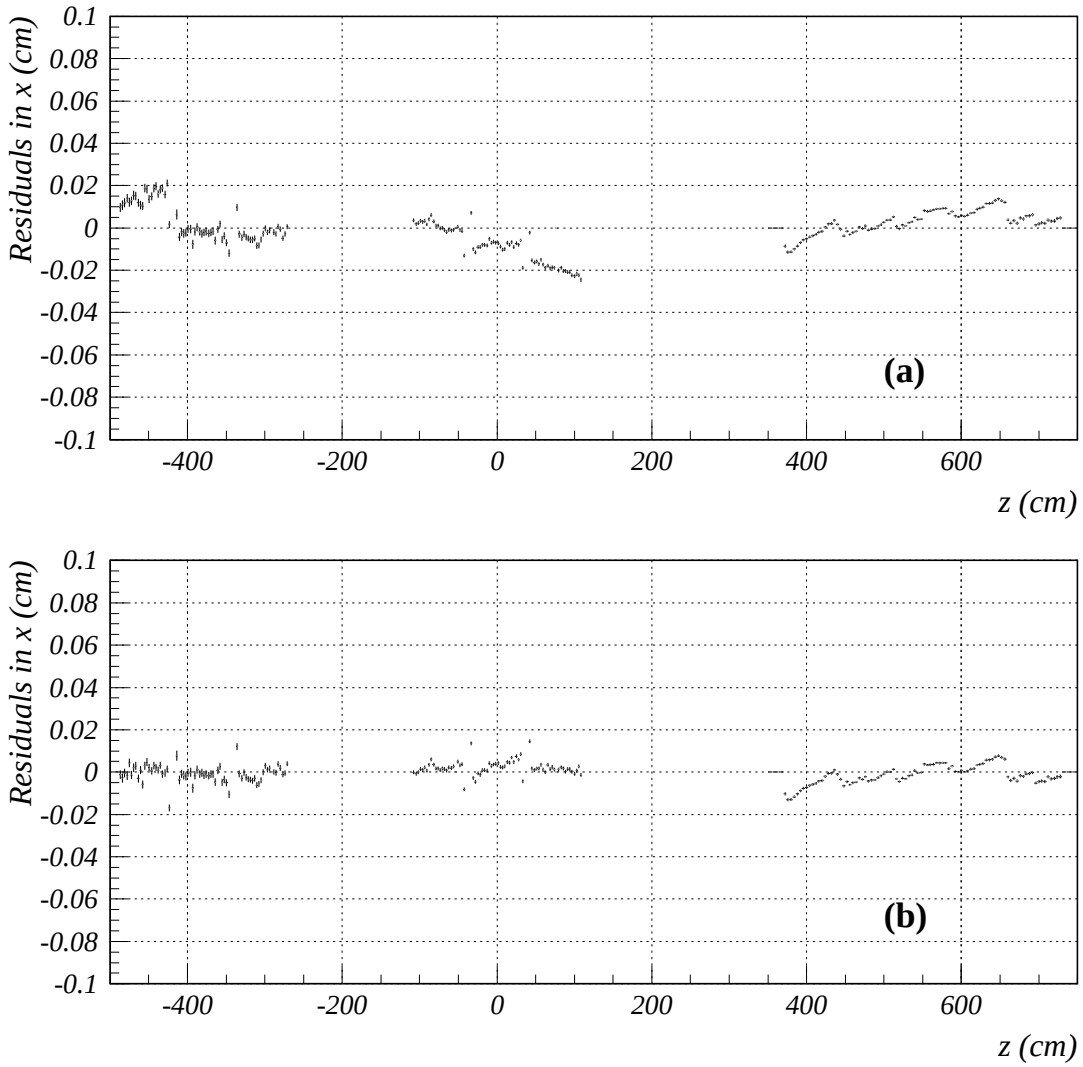

Figure 3: Average transverse residuals (B=0) for single global tracks (muon tracks parallel to the beam direction) with a) survey geometry only and b) detector alignment corrections.

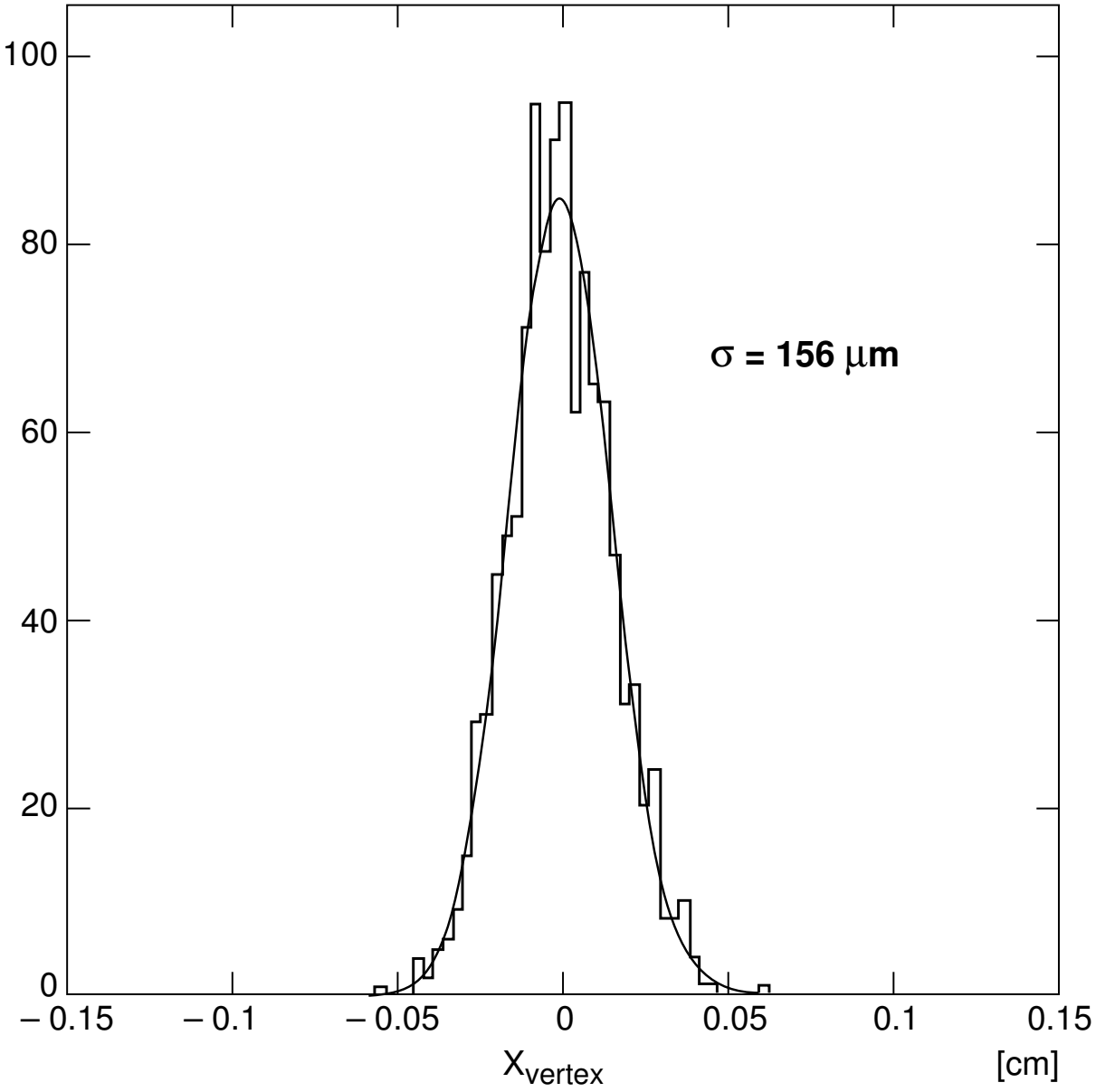

Figure 4: Position resolution of main vertex in transverse direction for particles produced in central Pb+Pb collisions at 158 A·GeV.

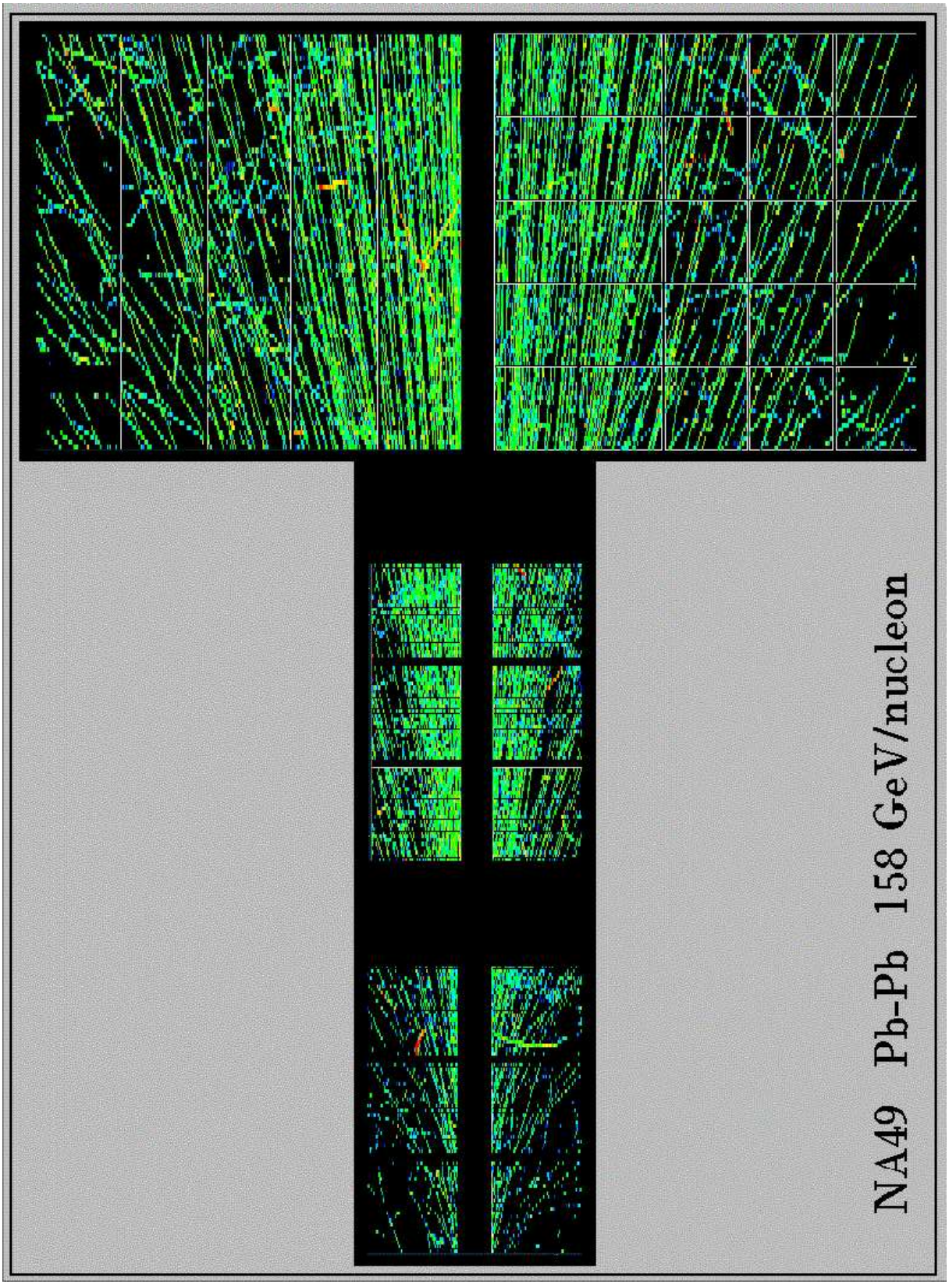

Figure 5: Top view of a 7 mm high horizontal slice around the beam plane for a central Pb+Pb event.

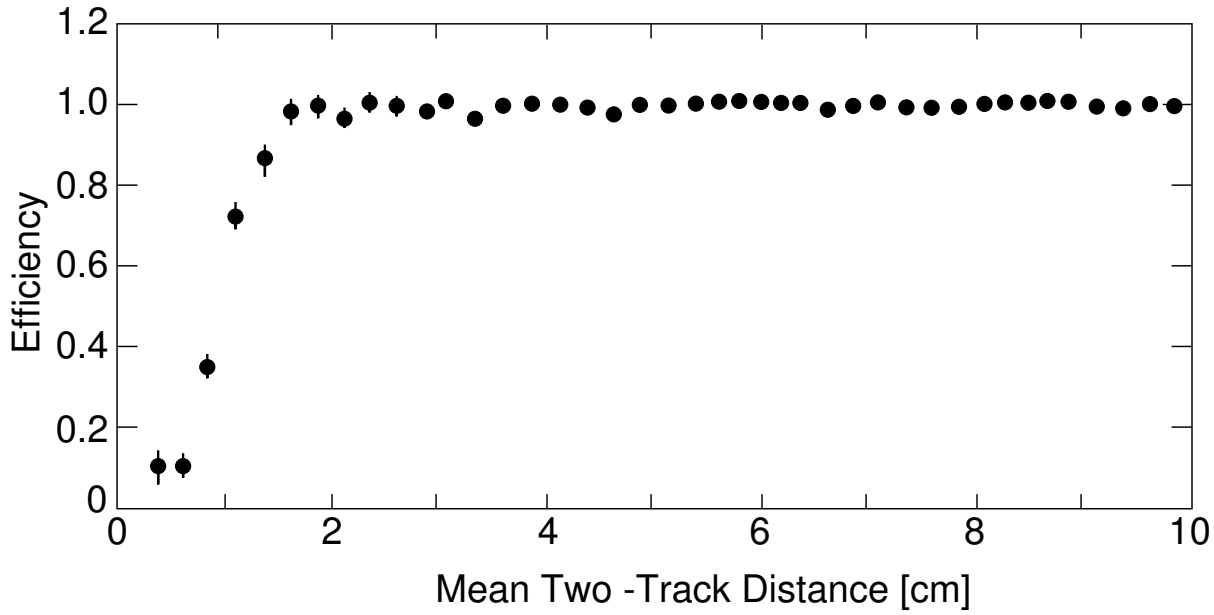

Figure 6: Track reconstruction efficiency in VTPC–2 as function of mean two–track distance revealing a two–track resolution of 1 cm (see text).

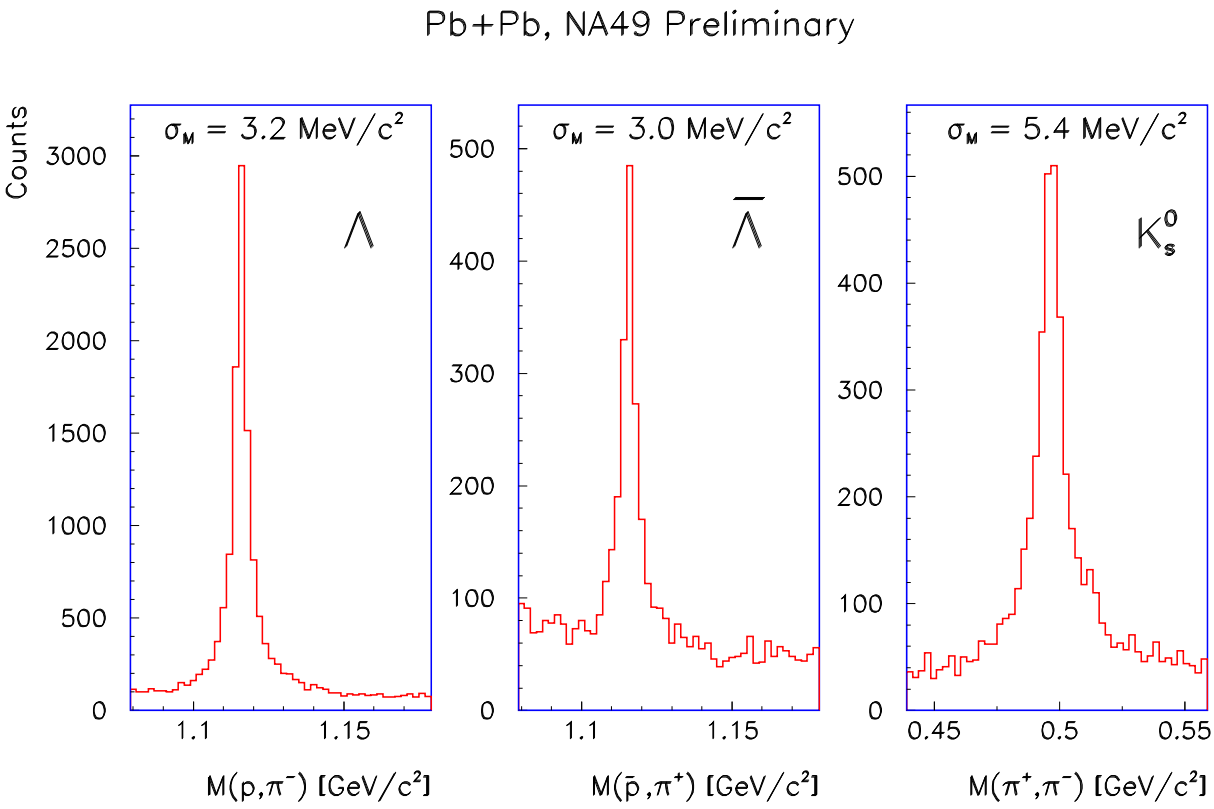

Figure 7: Invariant mass distributions for Λ, $\overline{\Lambda}$ and K^0_S produced in central Pb+Pb collisions at 158 A·GeV.

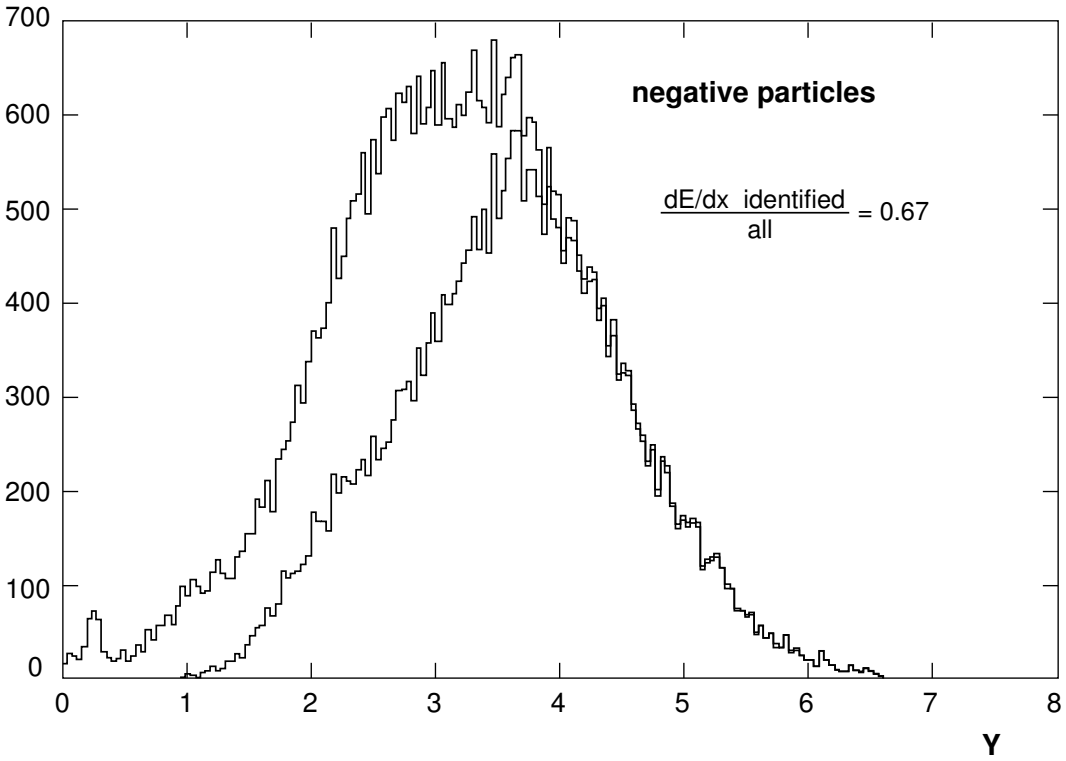

Figure 8: Comparison of negative particles identified via dE/dx (MTPC) to all detected negative particles.

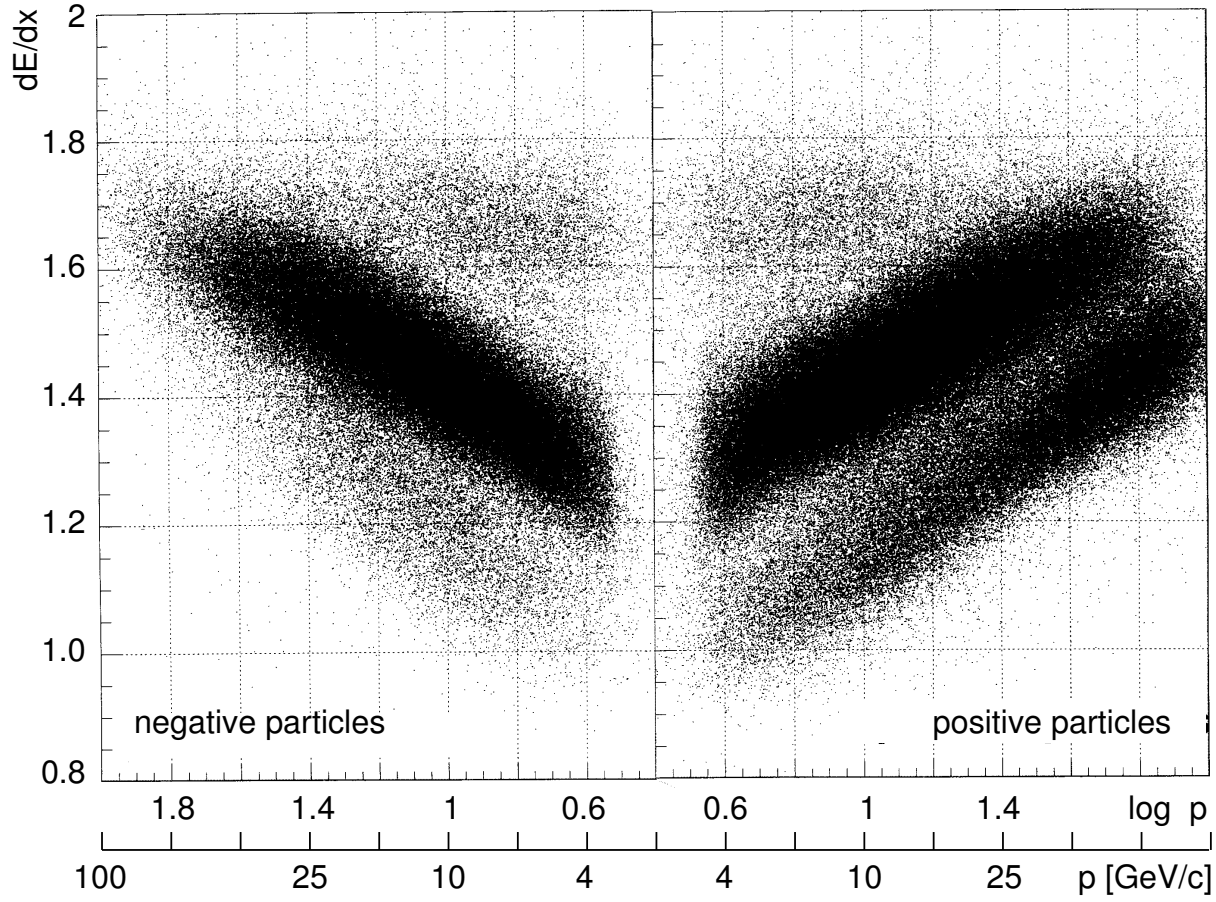

Figure 9: dE/dx measurement in $Ar/CO_2/CH_4$ (MTPC-L/R) as a function of momentum for particles produced in p+p interactions at 158 GeV/c.

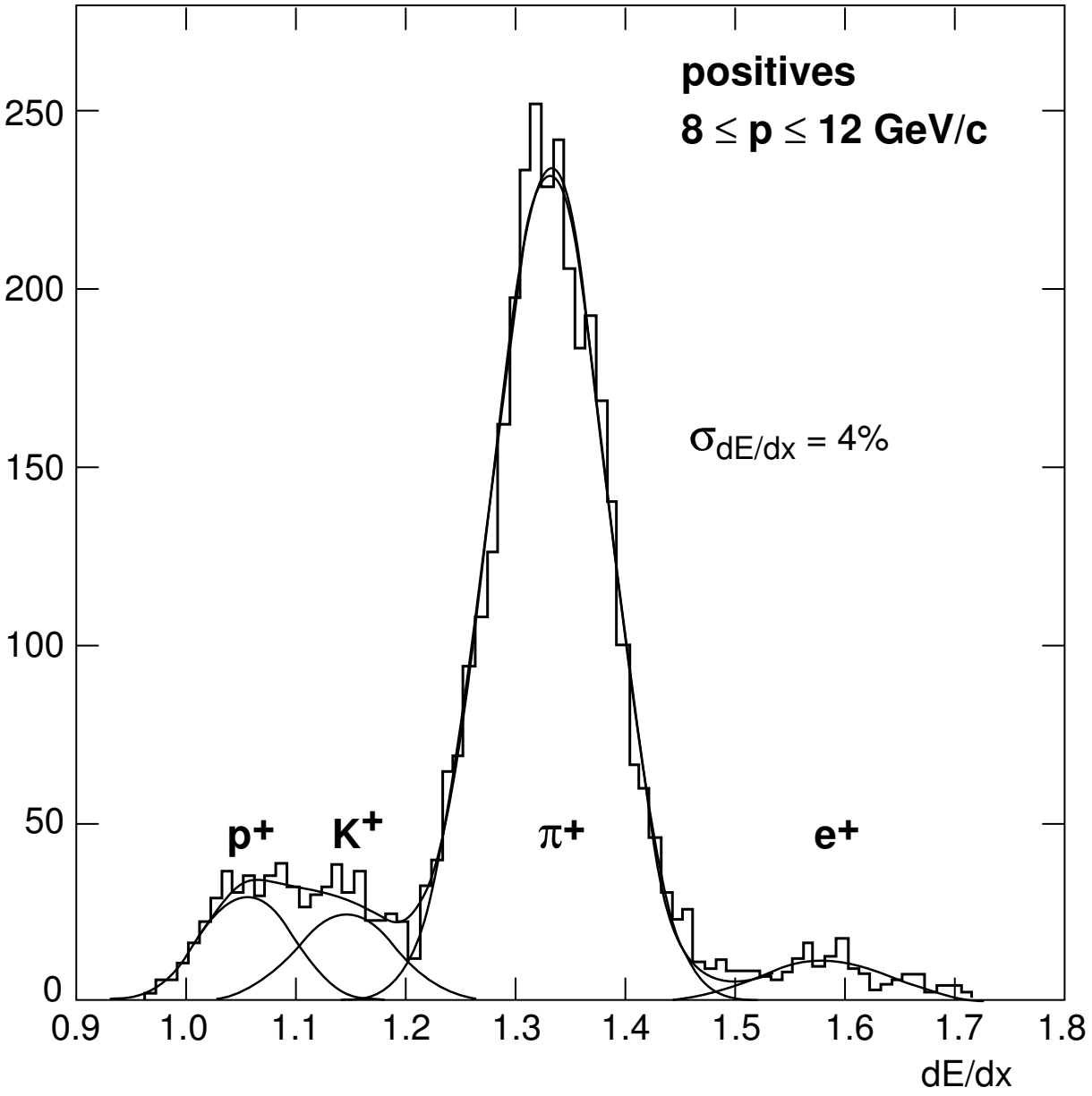

Figure 10: dE/dx distribution in the momentum bin 8–12 GeV/c for positive particles produced in p+p interactions at 158 GeV/c.

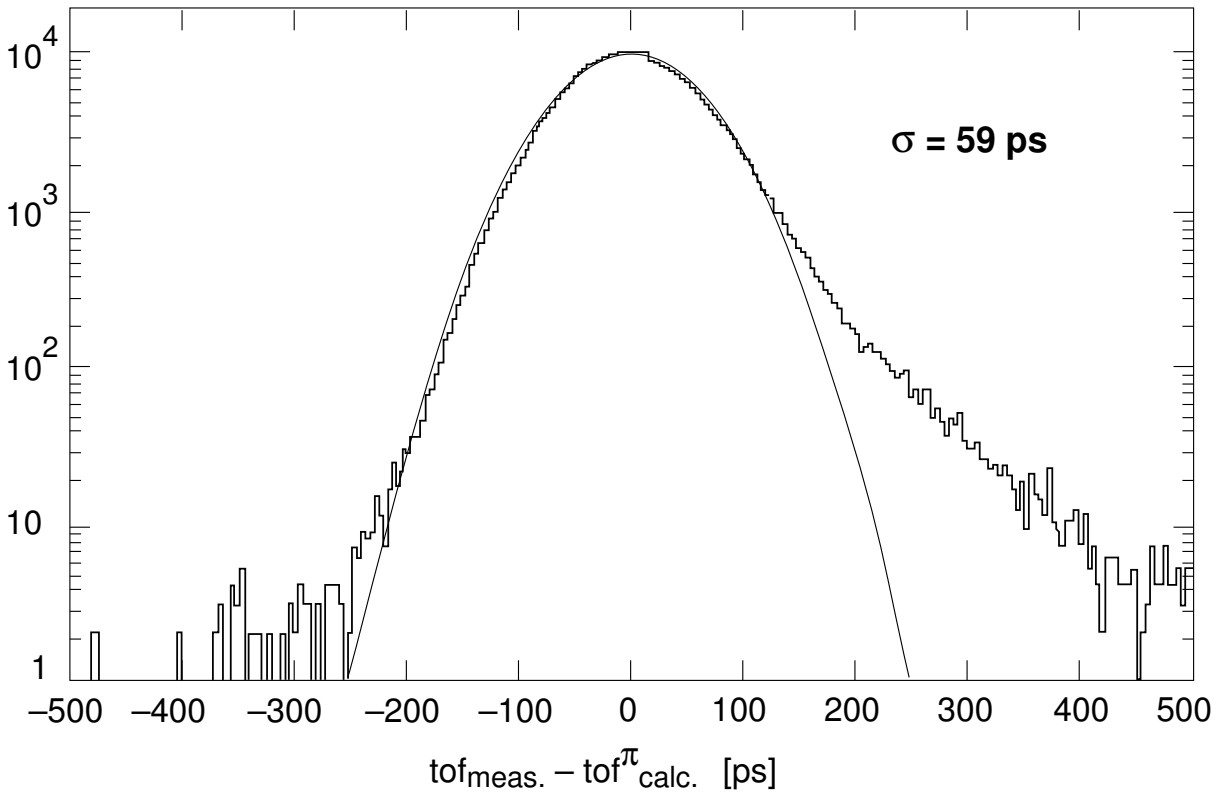

Figure 11: Difference between measured and calculated (assuming pion momentum) time–of–flight revealing a time resolution of 60 ps. The tail at large positive values is mainly due to conversion of background γ's in the scintillators.

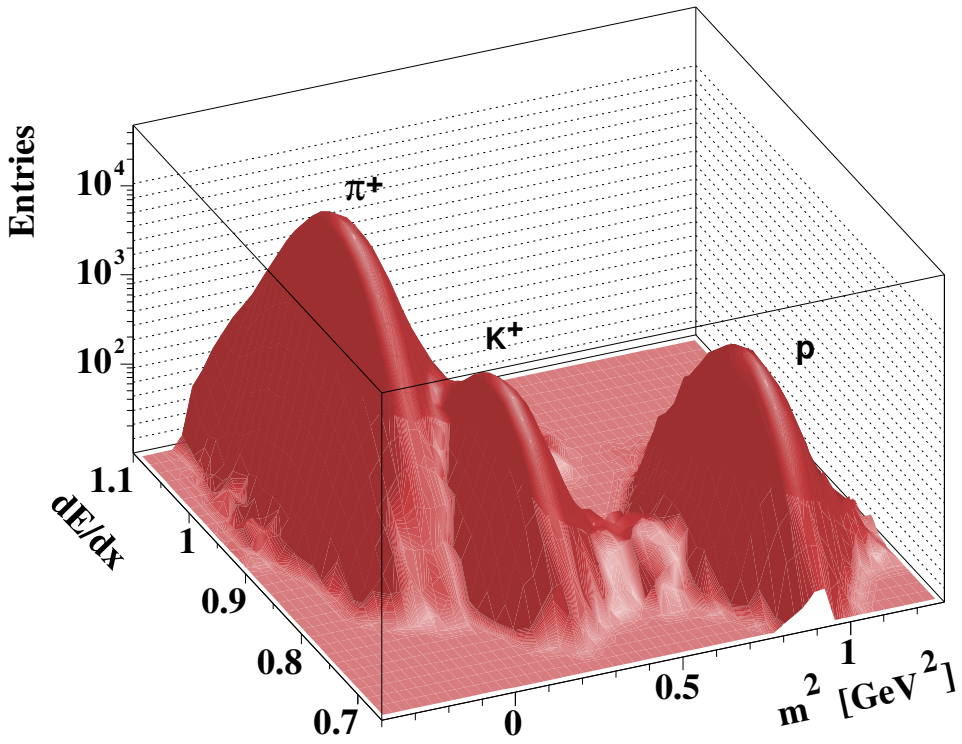

Figure 12: dE/dx measurement from MTPC vs. m^2 information from TOF in the momentum region 4–6 GeV/c for central Pb+Pb collisions at 158 GeV/c per nucleon.

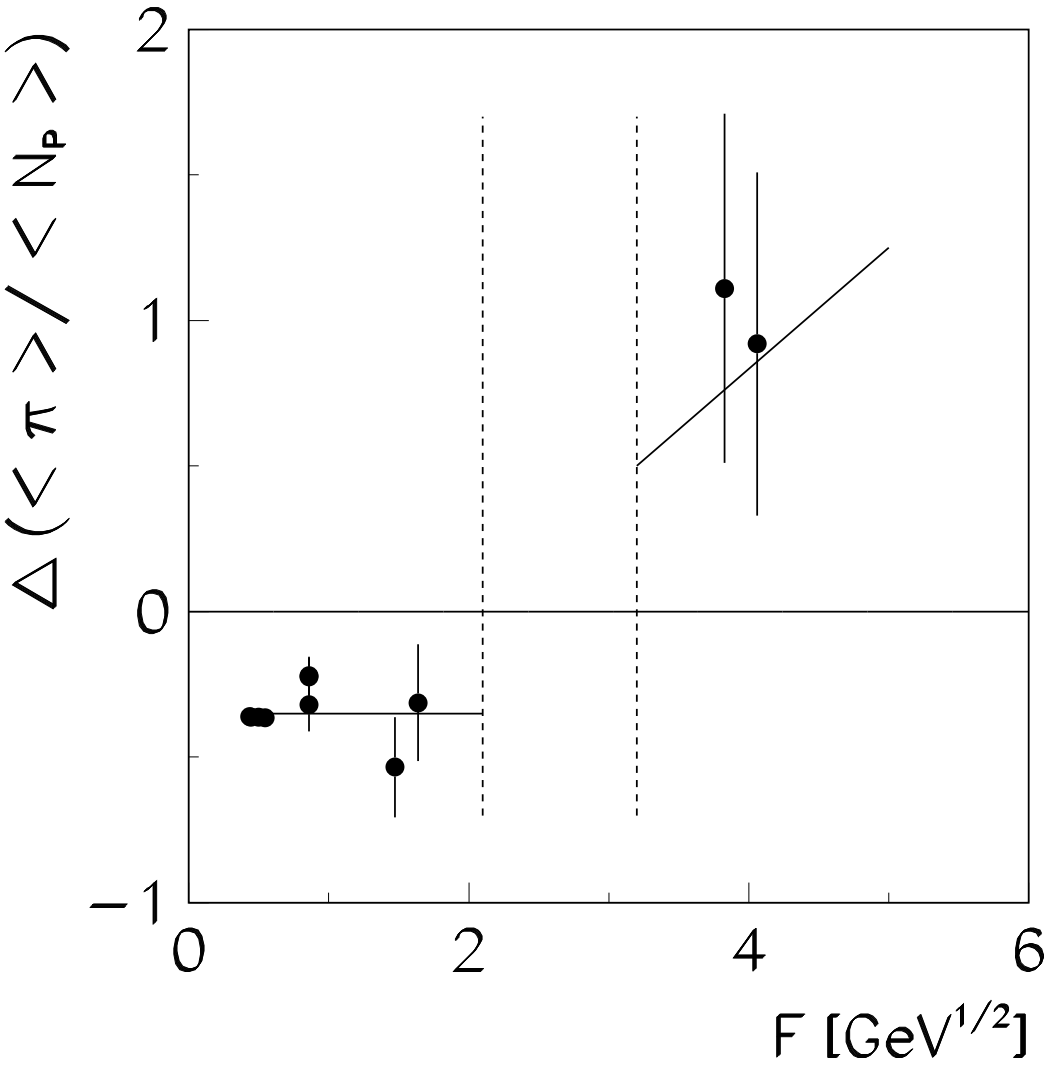

Figure 13: The dependence of the difference between pion/baryon ratios for central A+A collisions and nucleon–nucleon interaction at the same energy per nucleon on the collision energy [20] measured by the Fermi energy variable, $F = (\sqrt{s}_{NN} - 2m_N)^{3/4})/\sqrt{s}_{NN}^{1/4}$ [33]. The solid lines indicate the hypothetical energy dependence based on a generalized Landau approach [21] assuming transition to a deconfined partonic phase occuring in the energy region 30–80 A·GeV (dashed lines).

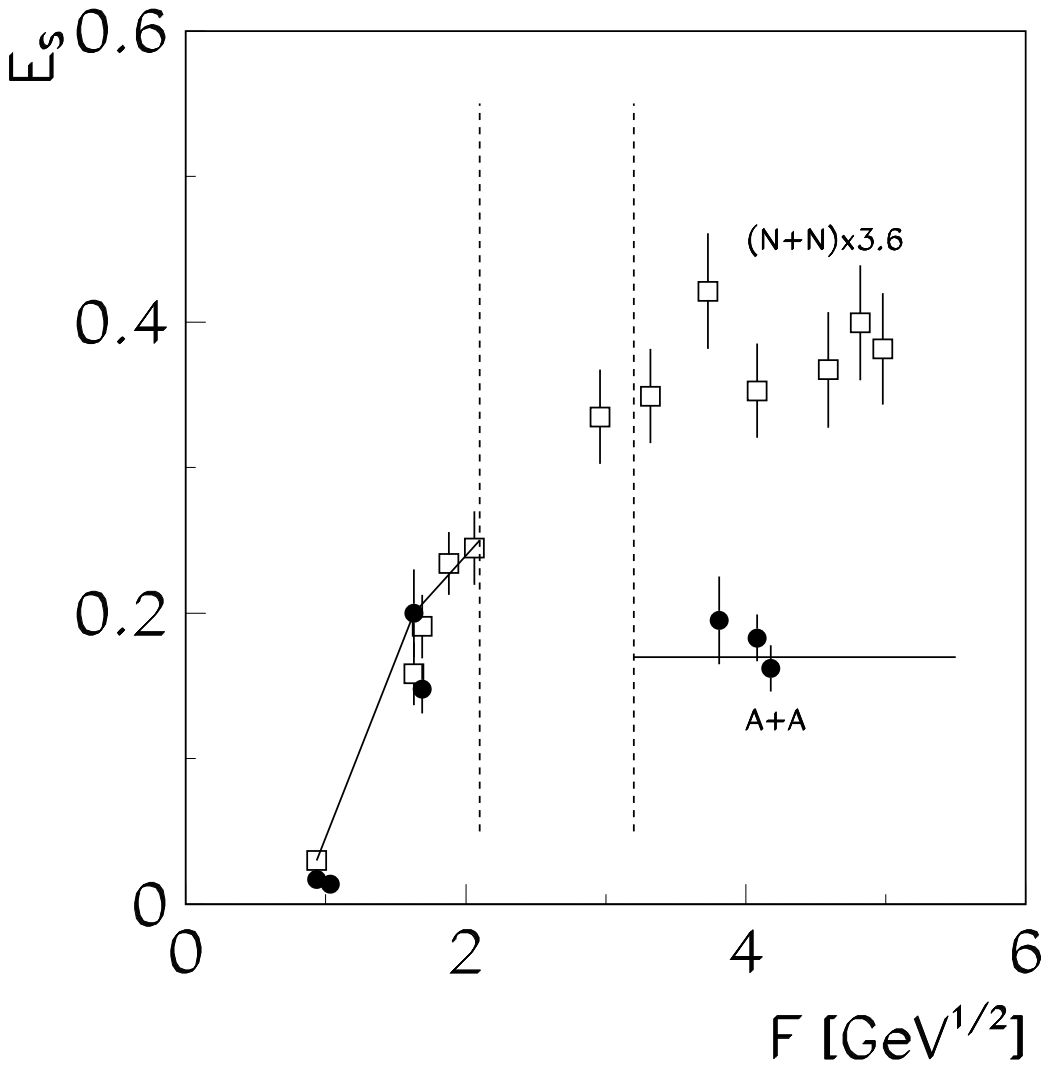

Figure 14: The dependence of the strangeness/pion ratio, $E_S = (\langle\Lambda\rangle+\langle K+\overline{K}\rangle)/\langle\pi\rangle$, for central A+A collisions (closed circles) and nucleon–nucleon interactions (open squares, scaled by a factor 3.6 to match A+A data at AGS energy) at the same energy per nucleon on the collision energy [20] measured by the Fermi energy variable, F. The solid lines indicate the hypothetical energy dependence based on the generalized Landau approach [21] assuming transition to a deconfined partonic phase occuring in the energy region 30–80 A·GeV (dashed lines).

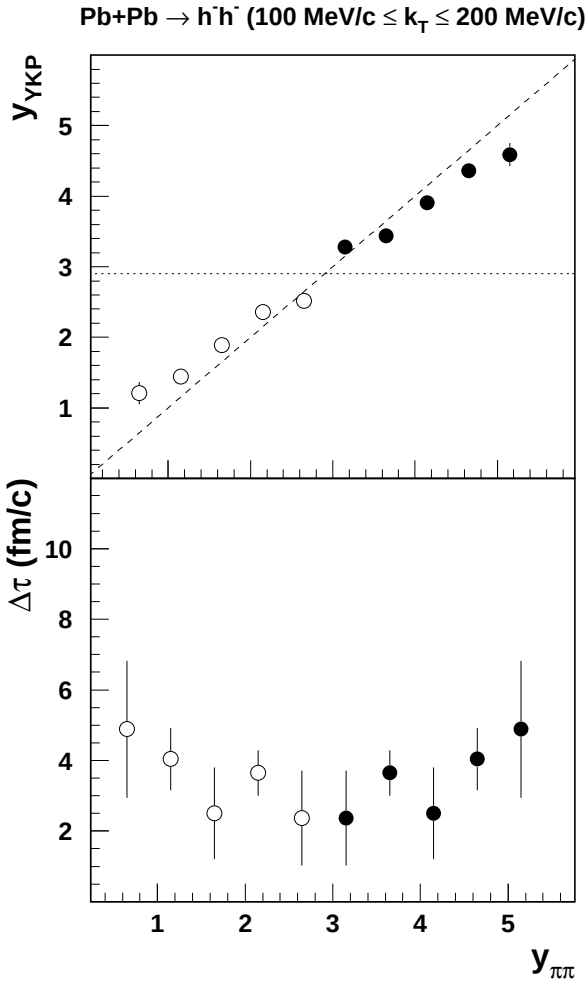

Figure 15: (a) Longitudinal flow rapidity y_{YKP} as a function of pion pair rapidity $y_{\pi\pi}$ for central Pb+Pb collisions at 158 A·GeV. The dashed line indicates the dependence of y_{YKP} on $y_{\pi\pi}$ for boost invariant expansion. The dotted line shows the dependence of y_{YKP} on $y_{\pi\pi}$ for a stationary source created at $y = y_{cms} = 2.9$ [5]. (b) Mean Gaussian width for the duration of pion emission $\Delta\tau$ as a function of pion pair rapidity $y_{\pi\pi}$ [5].

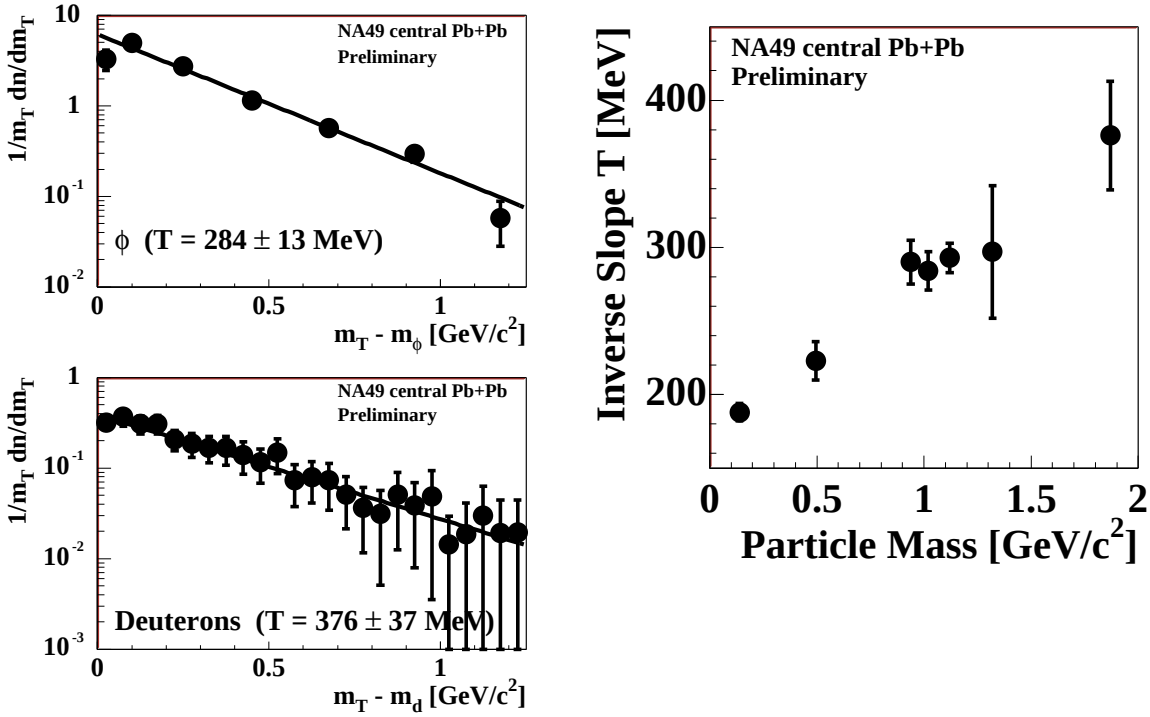

Figure 16: The transverse mass spectra of ϕ–mesons and deuterons produced in central Pb+Pb collisions at 158 A·GeV near midrapidity (left). The dependence of the inverse slope parameter, T, on the particle mass (π, K, p, ϕ, Λ, Ξ and d) for central Pb+Pb collisions at 158 A·GeV (right) [6].

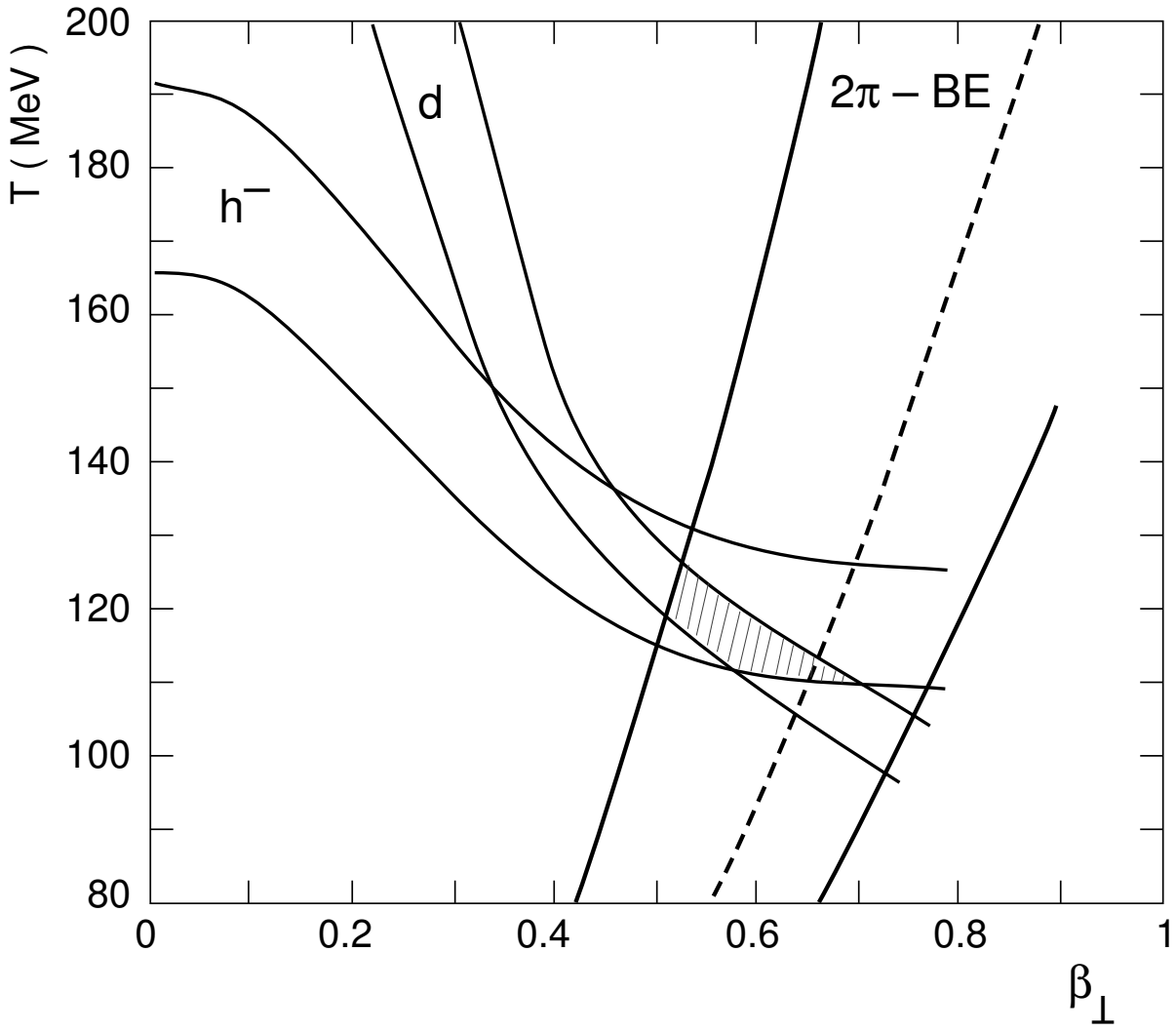

Figure 17: Allowed regions of thermal freeze–out temperature vs. radial flow velocity for central Pb+Pb collisions at 158 A·GeV near mid–rapidity derived from the negative hadron two particle correlation functions and from negative hadron and deuteron transverse mass spectra. Bands are drawn at $\pm\sigma$ around fitted values [5].
The overlapping region centers at $T = 120$ MeV and $\beta_T = 0.55$.

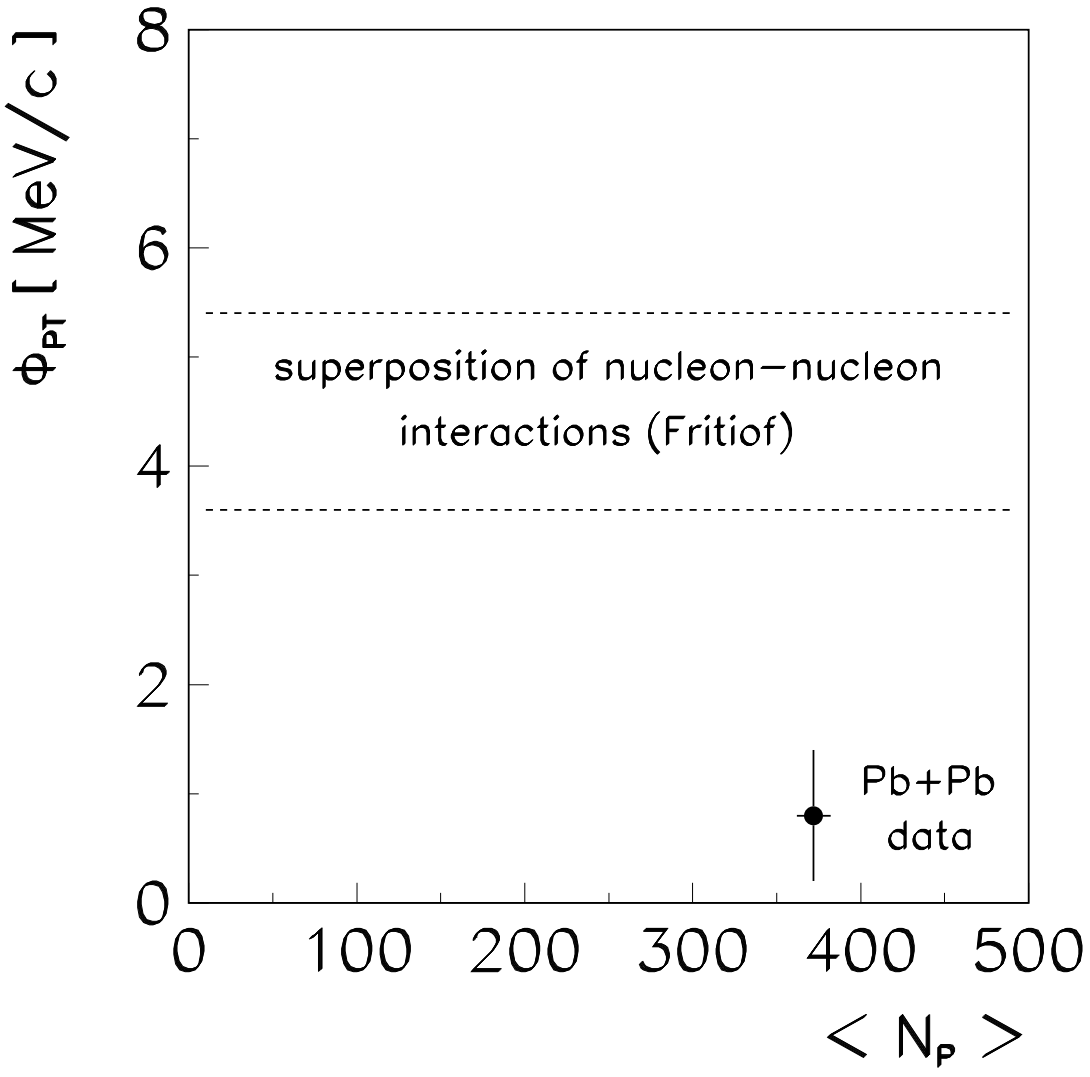

Figure 18: The measure of event–by–event fluctuations in transverse momentum Φ_{P_T} [24] as a function of the number of participant nucleons $\langle N_P \rangle$ [26]. By construction the value of Φ_{P_T} is equal to zero for independent particle emission from the dynamicaly identical collisions.

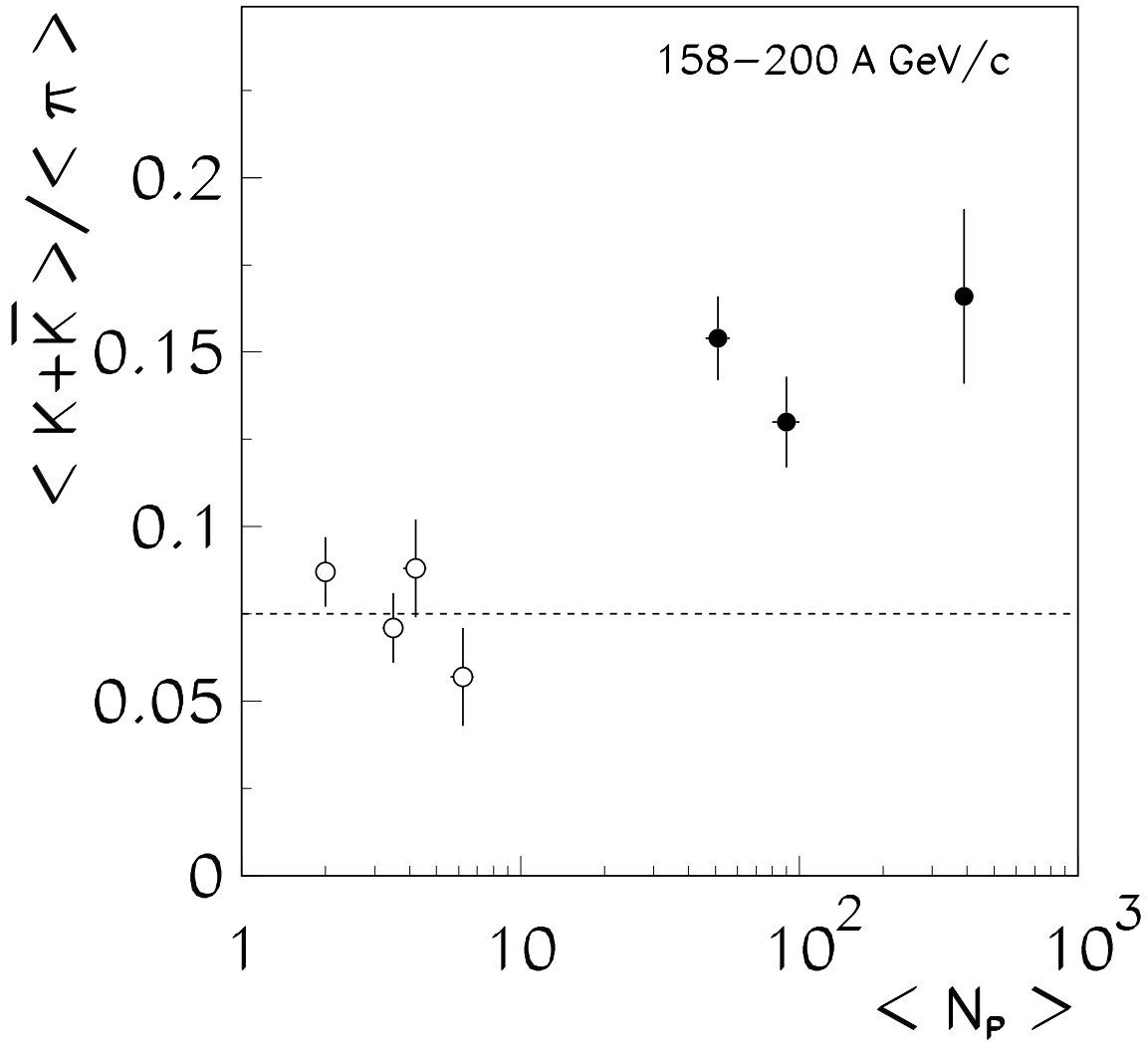

Figure 19: The dependence of the ratio of all produced kaons and antikaons to the total number of produced pions on the number of participants for p+A interactions (open circles) and central collisions of S+S, S+Ag and Pb+Pb at 158–200 A·GeV [27].

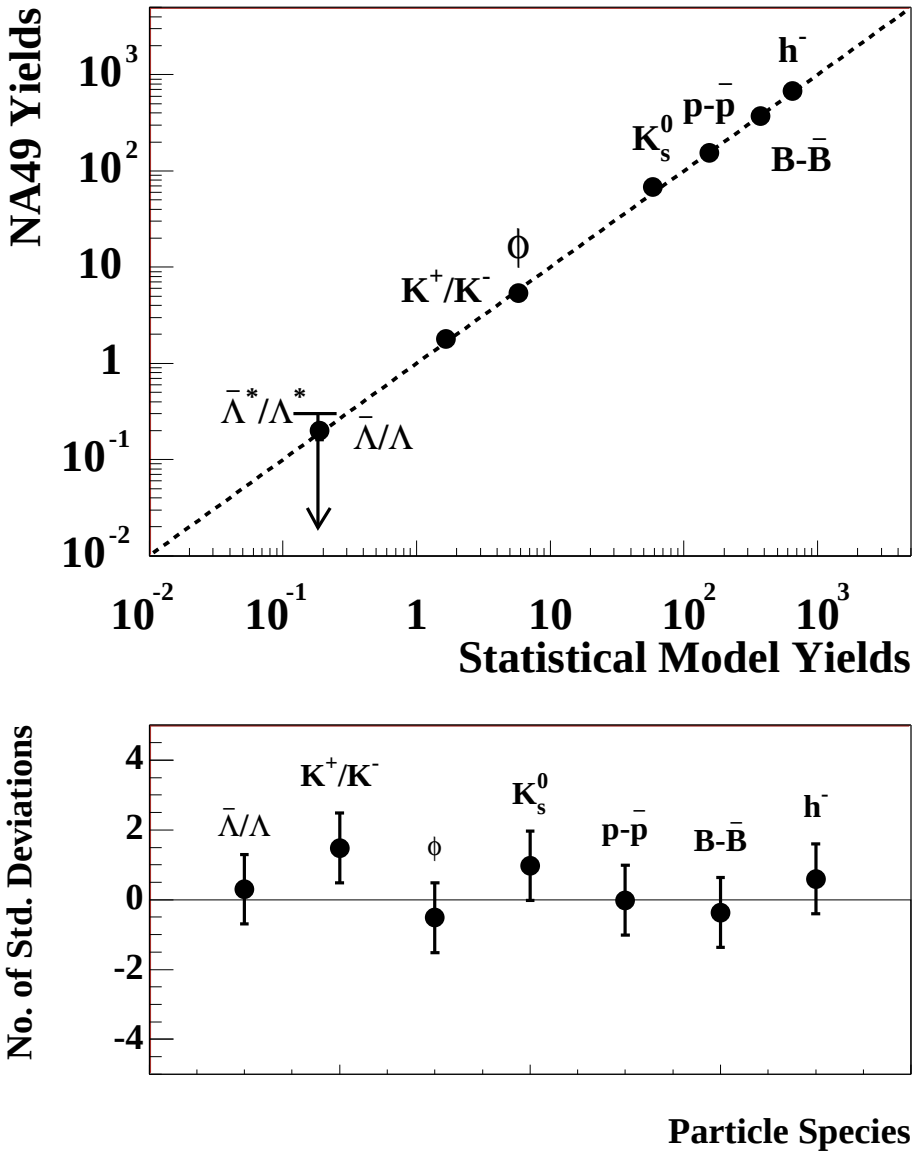

Figure 20: Comparison between the particle multiplicities measured by NA49 in central Pb+Pb collisions and the prediction of a statistical model [30]. The derived parameters of the chemical freeze–out are $T = 193$ MeV, $\mu_B/T = 1.21$, and a strangeness saturation factor $\gamma_S = 0.62$.

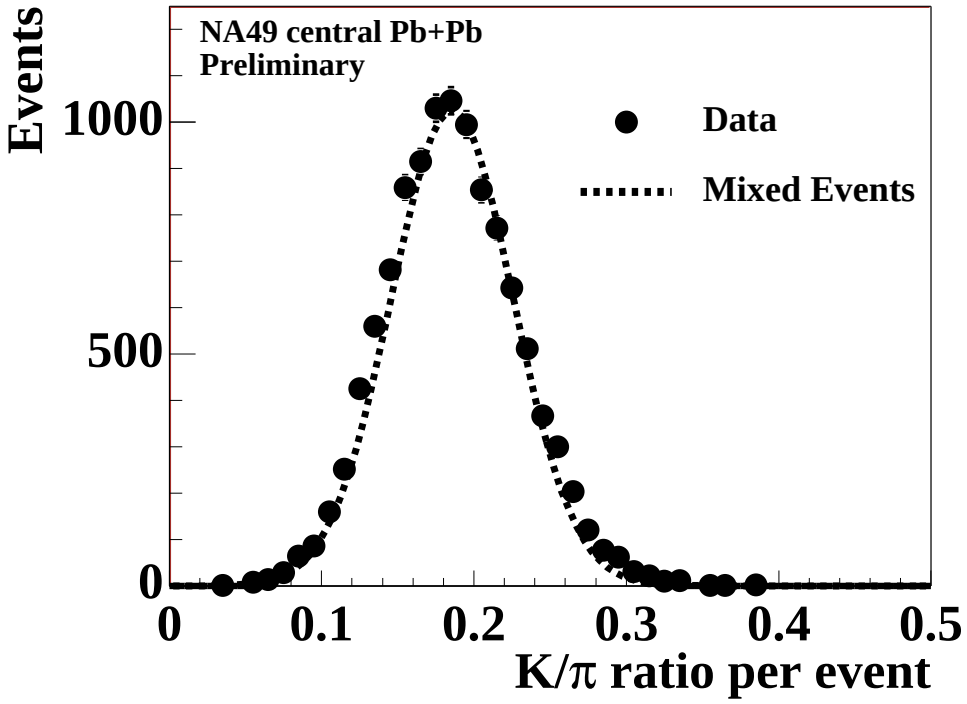

Figure 21: The event–by–event distribution of the K/π ratio for central Pb+Pb collisions at 158 A·GeV [6]. The data refer to the interval $4 < y < 5.5$. The dashed line shows a correlation-free reference distribution obtained from an analysis of so-called mixed events. The mixed events were created by combining particles randomly selected from different events.

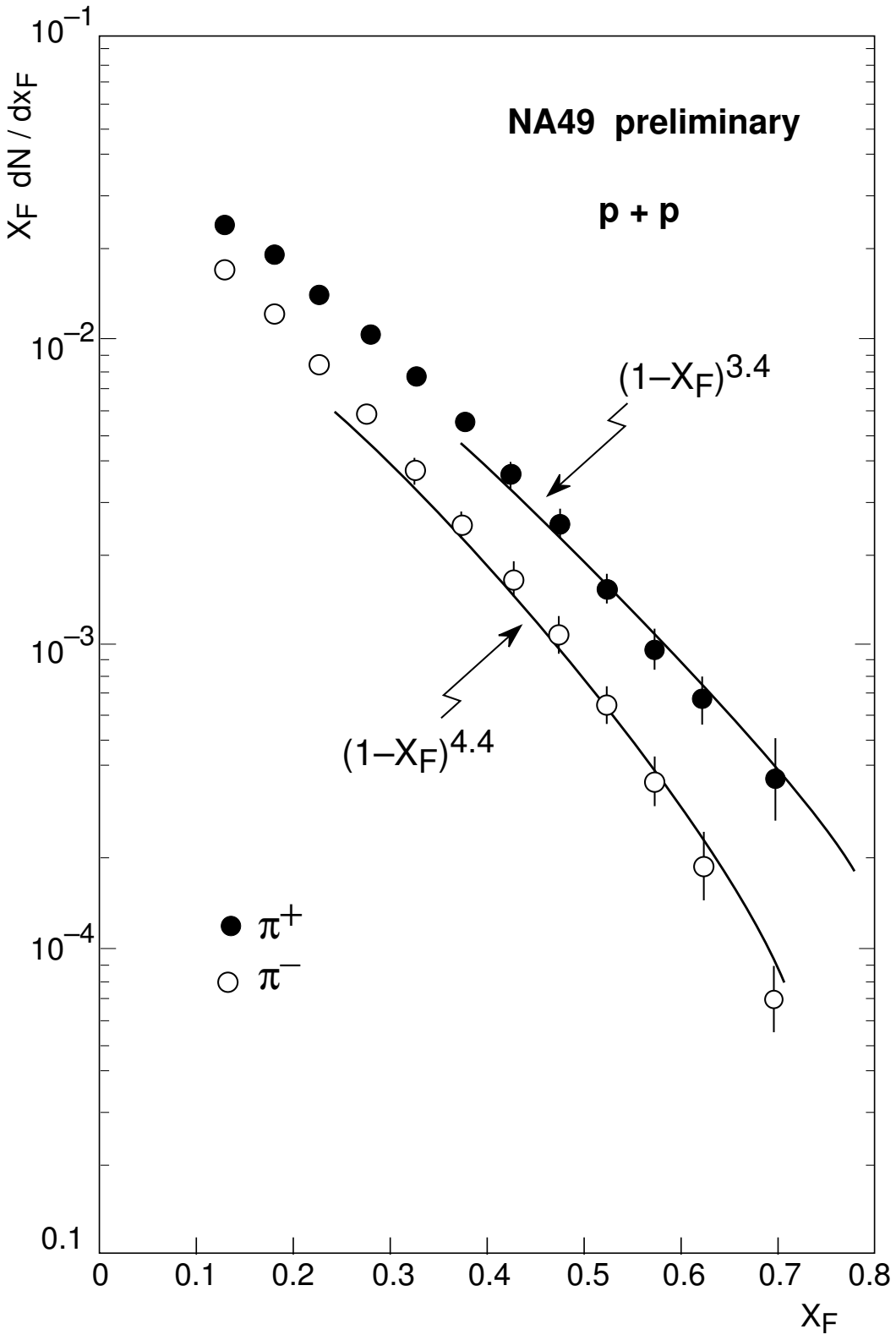

Figure 22: Invariant cross section as function of x_F for π^+ and π^- in minimum bias p+p events.

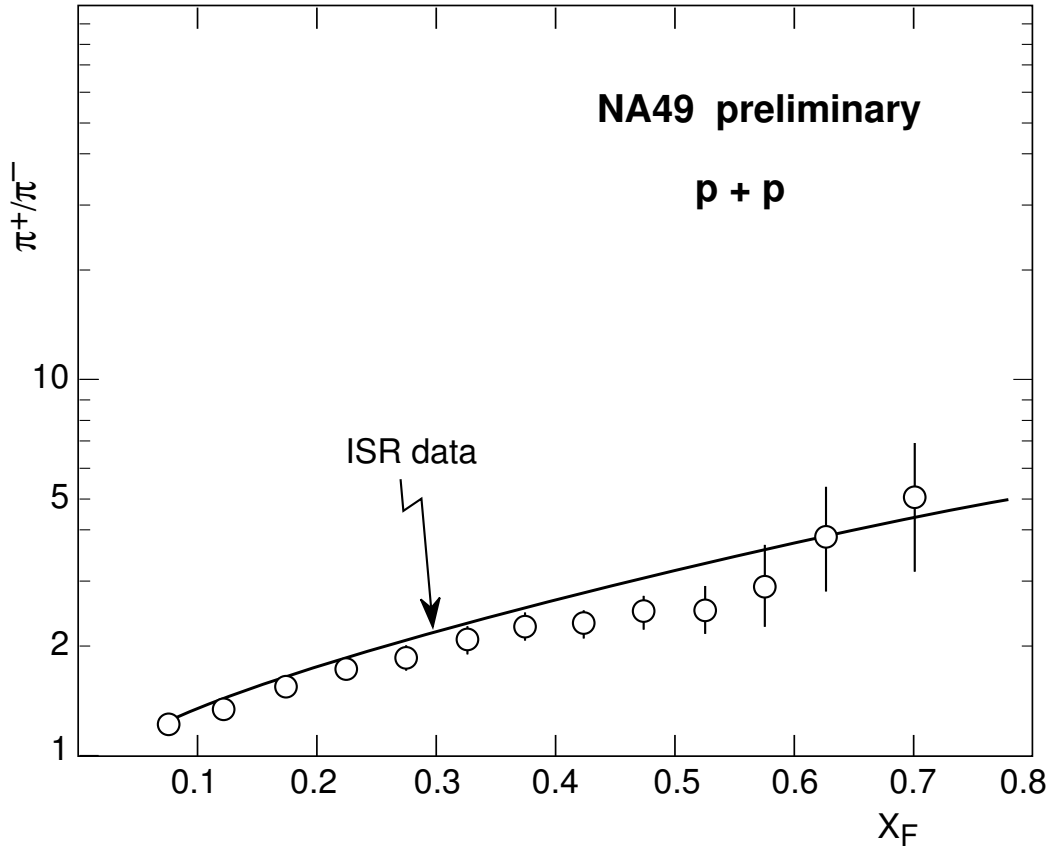

Figure 23: Charge ratio of π^+ and π^- as function of x_F, compared to ISR data.

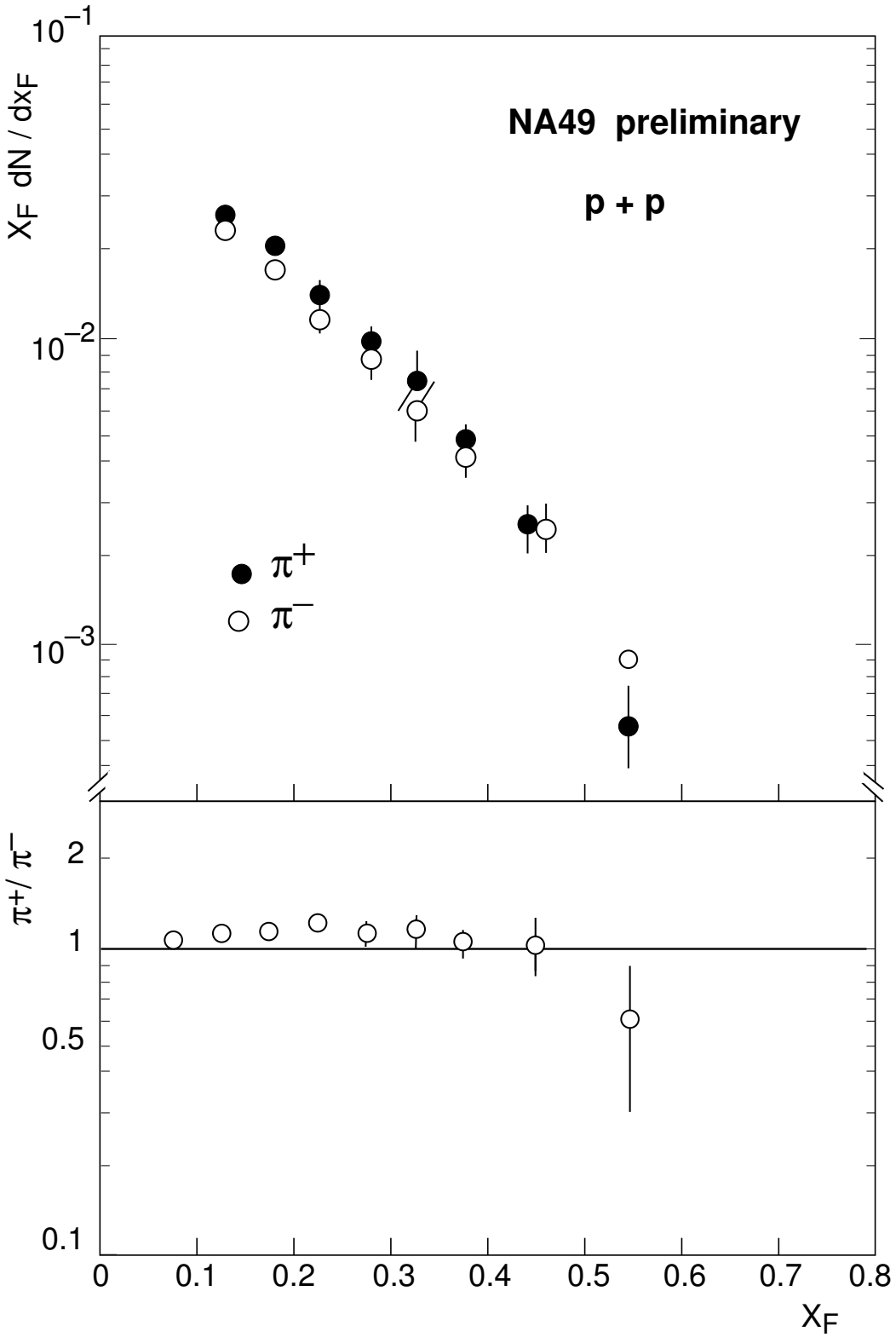

Figure 24: Invariant cross sections and charge ratios for π^+ and π^- as function of x_F, for p+p events with identified protons in the range $0.2 < x_F(\text{proton}) < 0.5$.

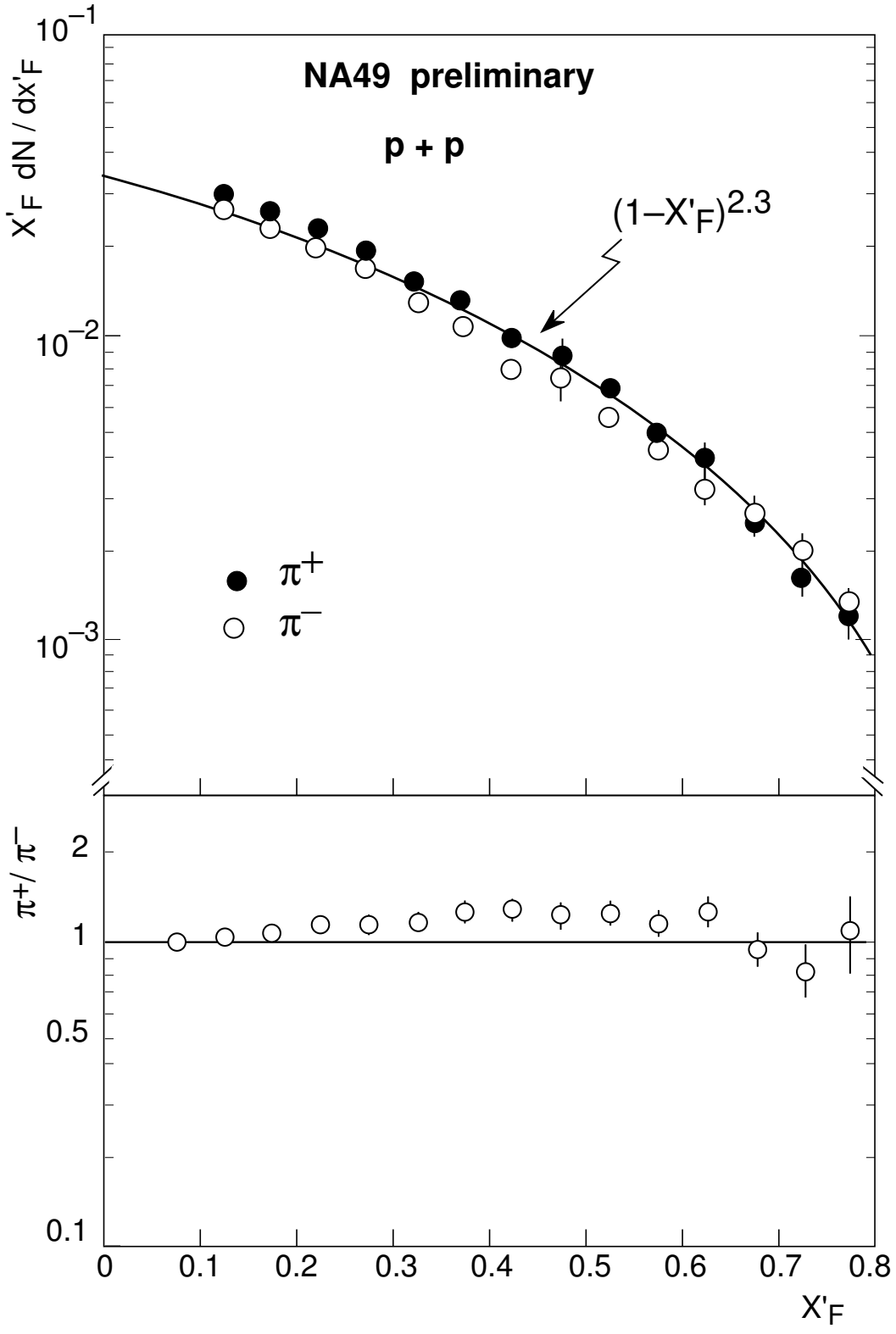

Figure 25: Same as Fig. 24 but with redefined longitudinal momentum scale, $x'_F = x_F/(1 - x_F(\text{proton}))$.

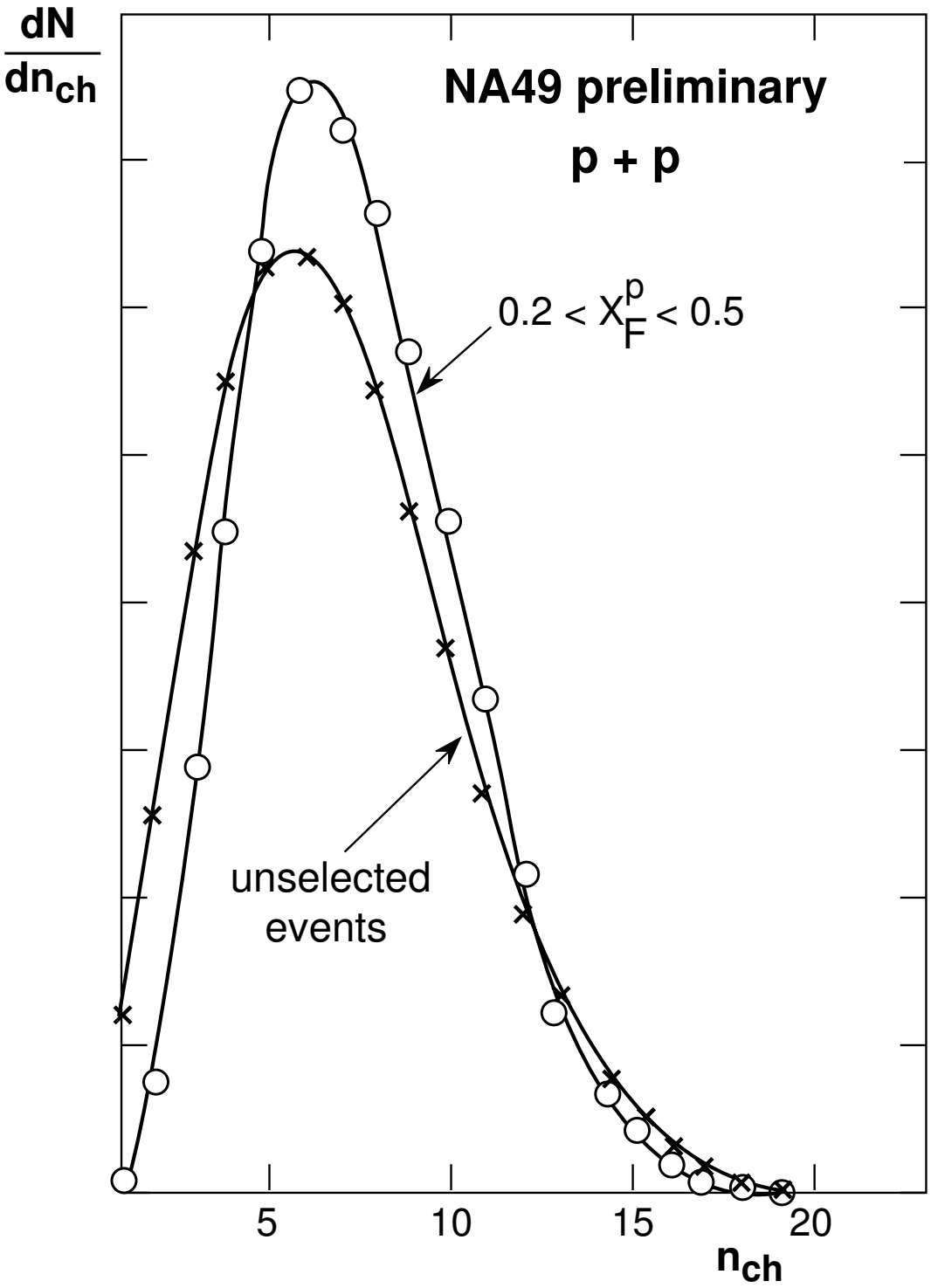

Figure 26: Charged multiplicity distribution for minimum bias events (crosses) and events with protons in the range $0.2 < x_F(\text{proton}) < 0.5$ (open circles). The distributions are normalized to the same surface.

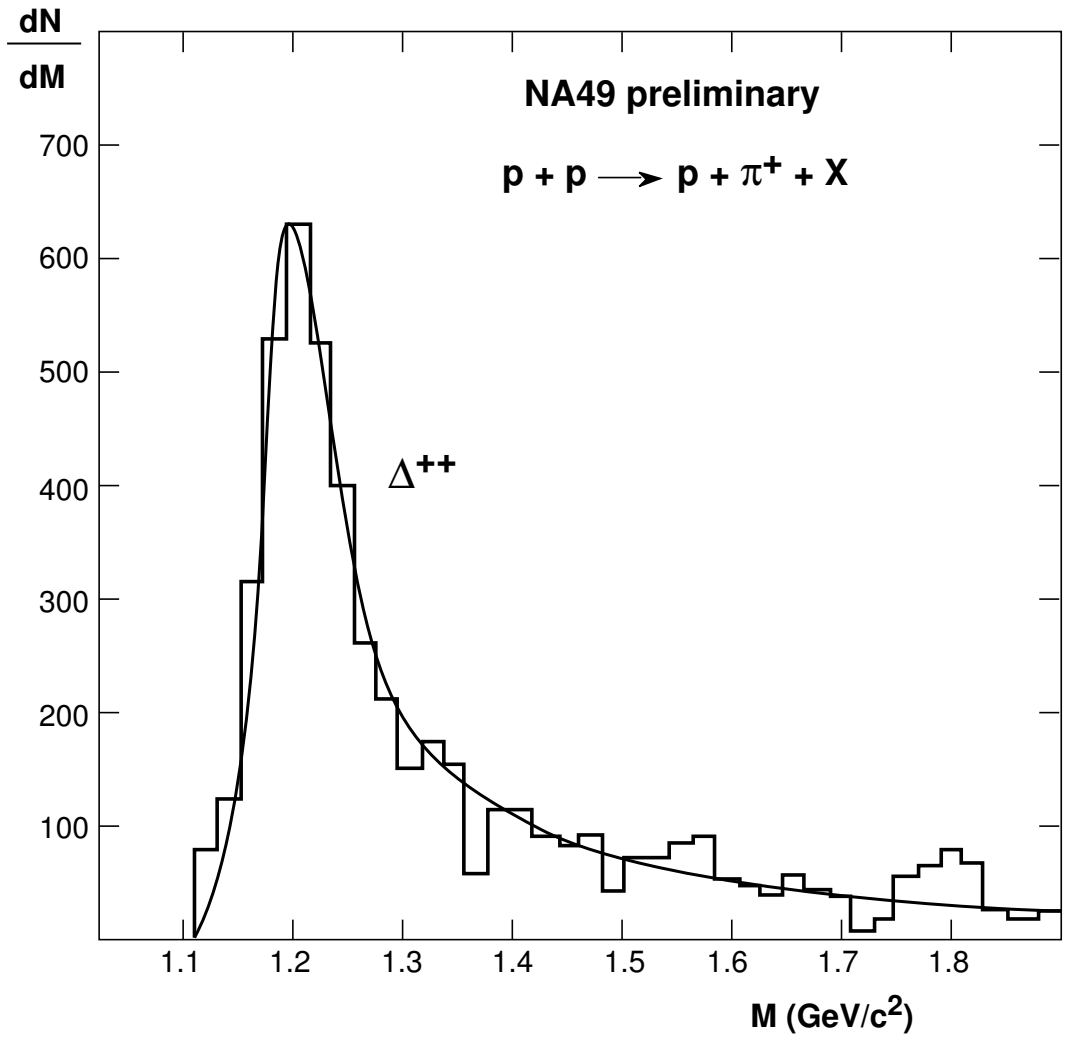

Figure 27: Background–subtracted mass distribution of p+π^+ mass combinations with $0.2 < x_F(\text{proton}) < 0.5$. The full line is a relativistic Breit–Wigner function.

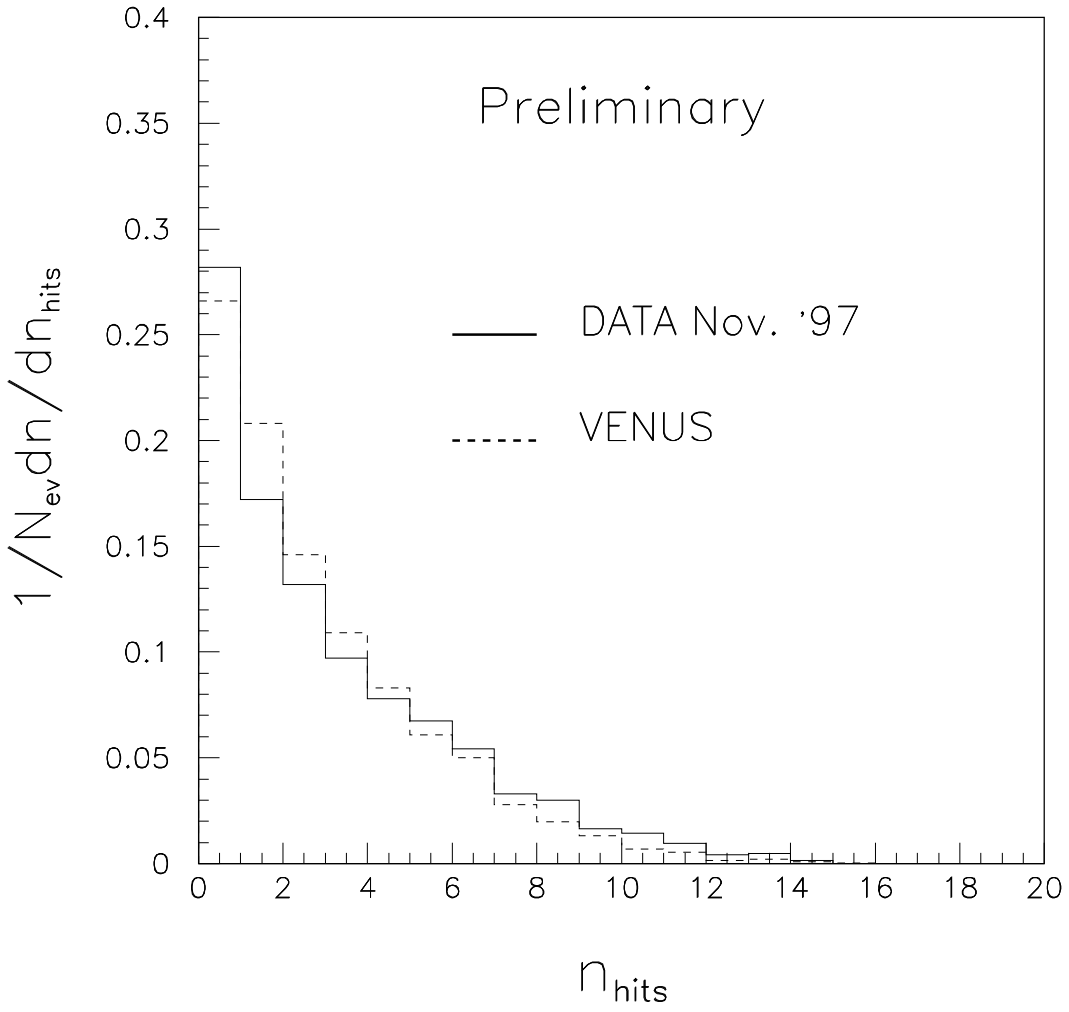

Figure 28: Number distribution of hits in the NA49 centrality detector using unselected p+Pb events. The hatched line shows a prediction using the VENUS event generator folded with the acceptance of the detector.

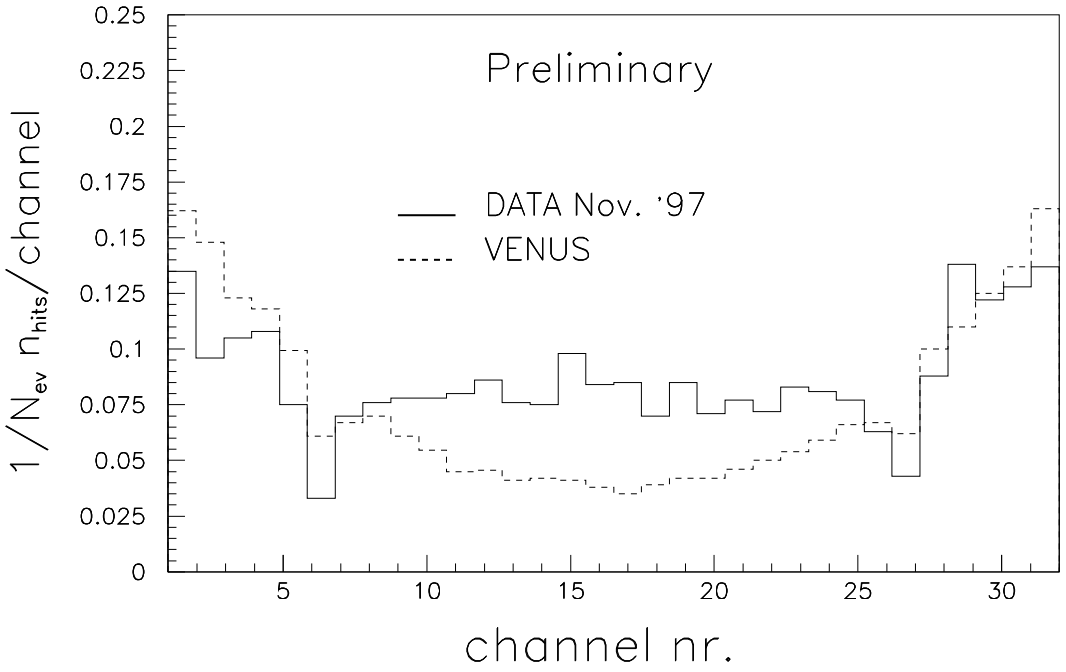

Figure 29: Polar angle distribution of centrality detector hits compared to the VENUS simulation code. Channel 1 and 32 correspond to polar angle $\pm$ 45 degrees, channel 16 to 180 degrees.

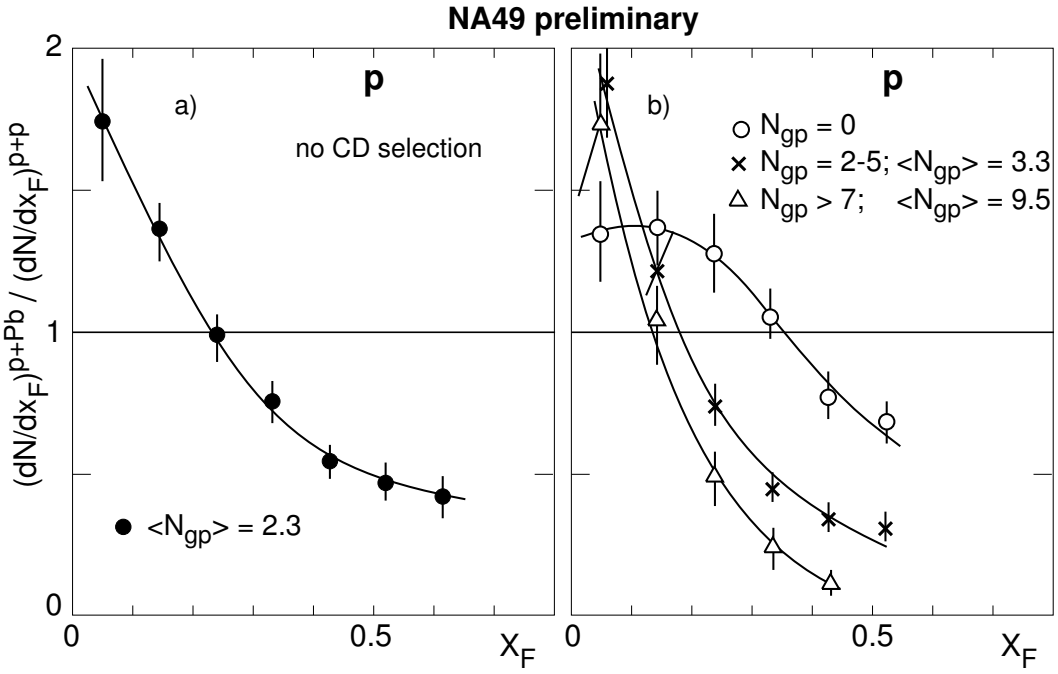

Figure 30: Ratio of particle densities (protons) of p+Pb and p+p events as function of x_F for a) unselected events and b) events selected in bins of "grey" proton counts N_{gp}.

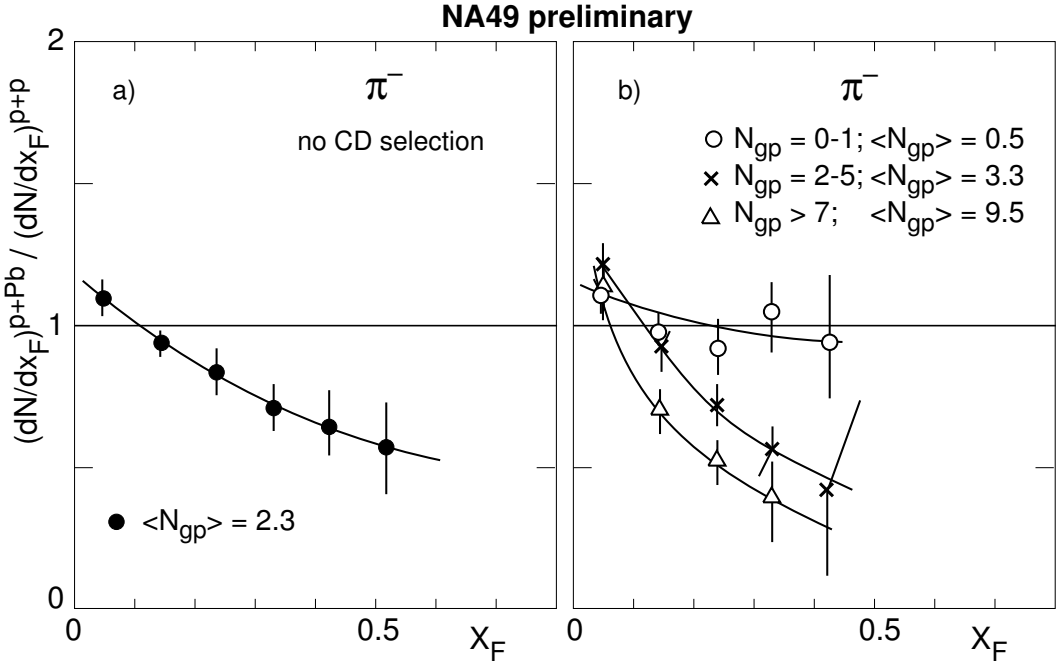

Figure 31: Ratio of particle densities (π^-) of p+Pb and p+p events as function of x_F for a) unselected events and b) events selected in bins of "grey" proton counts N_{gp}.